2020

Indoor Navigation for Visually Impaired Person Using Inertial and Geomagnetic Information

Jayanth Ammanabrolu
Minnesota State University, Manakto

Indoor Navigation for Visually Impaired Person Using Inertial and Geomagnetic Information

By

Jayanth Ammanabrolu

A Thesis Submitted in Partial Fulfillment of the

Requirements for the Degree of

Master of Science

In

Mechanical Engineering

Minnesota State University, Mankato

Mankato, Minnesota

July 2020

3/30/2020

Title: Indoor Navigation for Visually Impaired Person using Inertial and Geomagnetic information

Name: Jayanth Ammanabrolu

This thesis has been examined and approved by the following members of the student's committee.

_____

Dr. Min Li

Advisor

_____

Dr. Khosrow Ebrahimi

Committee Member

_____

Dr. Kuldeep Agarwal

Committee Member

Acknowledgments

Entering into an era of autonomous wayfinding for many applications, I am really glad that I have chosen this topic that relates closely. This project has not been so easy, and I would like to thank Dr. Min Li for his continuous assistance and support throughout my project. Dr. Li has provided his perception and expertise that critically assisted this research. I also thank my committee members, Dr. Ebrahimi Khosrow and Dr. Kuldeep Agarwal, for their advice and research tips. I dedicate this thesis to my mom, dad and sister for their continuous love and support throughout my tough times.

.

Table of Contents

List of Figures

List of Tables

Indoor Navigation for Visually Impaired Person Using Inertial and Geomagnetic Information

Jayanth Ammanabrolu

A thesis submitted in partial fulfillment of the

requirements for the degree of

Master of Science in Mechanical Engineering

Minnesota State University, Mankato

Mankato, Minnesota

July 2020

Abstract

Motivated by the need for assistance of indoor guidance for visually impaired persons (VIPs), a sensing system using inertial and geo-magnetic information has been developed to navigate a VIP person indoor. Orientation estimation, which is critical for indoor localization, is conducted using the information of the angular velocity, acceleration and geomagnetic field. By analyzing the characters of human gait, a method to eliminate the accumulated drift introduced by double integrations is introduced. By attaching the inertial sensor to the foot, the periodic stationary state will facilitate the drift correction. Also, the distinctive distortion of the geomagnetic field, which contains spatial information, provides a good approach to estimation location by utilizing an improved subsequence Dynamic Time Warping (DTW) Algorithm. To eliminate the effect of the relative constant geomagnetic field, magnetic tensor is introduced to extract the magnetic distortion. Kalman filter is utilized to fuse the orientation and location estimations of respective inertial and geomagnetic information and provide reliable and accurate indoor location. To demonstrate the accuracy and efficiency of the newly designed algorithms and sensing system, a prototype which consists of inertial sensors and magnetic tensor sensor was developed. Several experiments with three different indoor routes were designed to demonstrate and illustrate the sensing system.

Chapter 1. Introduction and Background

1.1 Introduction

Human relies on the vision systems to percept and interpret their surroundings. Estimated in 2010, globally there were 285 million visually impaired people, of whom 39 were blind. Most of them live in developing countries [1]. For people who lost the visual ability, way-finding, which is an easy task for healthy people to navigate indoor and outdoor, becomes a challenging and daunting task.

Traditionally, several methods have been utilized to assist the visually impaired person (VIP) to find a way, such as tactile paving, white canes and guide dogs. Tactile paving is a system of textured ground surface indicators designed to assist the VIPs to find the way and avoid obstacles. As part of infrastructures, it is not practical to promote tactile paving in the developing countries where most of VIPs live and have this indicator system installed everywhere (indoor and outdoor). White canes are one of the most widely used tools to assist the VIPs for wayfinding due to the low cost, lightweight and small size. The VIPs feel confident about the information they percept from the white canes. By keeping scanning the limited areas ahead of the VIPs, they can only detect the sufficiently large obstacles (such as steps and uneven surface) near the ground/floor level. Guide dogs are another efficient method to assist the VIPs. However, it is very expensive to train a qualified guide dog, which can only serve for 5 years. Also, to take care of the guide dogs is not an easy task, especially for the VIPs. Traditional methods are not practical and efficient, which

leads to a high demand for new technologies/methods to guide the VIPs and facilitate their daily life.

Although very high-resolution images are now widely available at low cost, optically obtained images must be processed digitally and converted into some other forms (such as voice and tactile) before they can be effectively appreciated by the visually impaired. Among the key challenges for a visually impaired person to effectively use existing vision algorithms (that are often designed for machine applications) is the lack of physical characteristics of objects in optically obtained images. Some other technologies like Wi-fi, Bluetooth and RFID have been used for indoor localization discussed in detail in section1.3. However, they do bring some disadvantages like infrastructure, time and accuracy. Thereby, a newly designed sensing system capable of assisting the VIPs for indoor navigation accurately and efficiently is highly desired.

1.2 Introduction to Inertial and Magnetic Sensors

Based on the sensor functionality, sensors can be divided into two categories, active sensors and passive sensors. An active sensor measures and retrieves the information of the physical quantity with the use of self-generated signals, such as LiDAR, ultrasonic, sonar etc. A passive sensor measures a naturally-generated physical quantity (or parameters) indicating object information and properties, such as gravity, light, temperature, magnetic field etc. Examples of passive sensors are thermocouple, geomagnetic sensor, optical sensor, Infrared sensor and inertial measurement unit (IMU) etc.

In this research, the primary sensors making use of naturally generated signals include micro-electromechanical system (MEMS) IMU (containing Gyroscope and Accelerometer) and MEMS Magnetometer sensors. A detailed sensor design for the newly designed sensing system is presented in Chapter 3.

1. MEMS Gyroscope

It has a proof mass resonating in one direction. According to newtons law a body continues to rotate in the direction of motions until an external force is acted upon it. When the resonating gyro mass is rotated, it deviates from its regular path by Coriolis effect. This is taken as an electrical signal which gives a measure of angular velocity of the object attached to the gyroscope. Figure 1 [2] illustrates a simplified structure of a MEMS gyroscope.

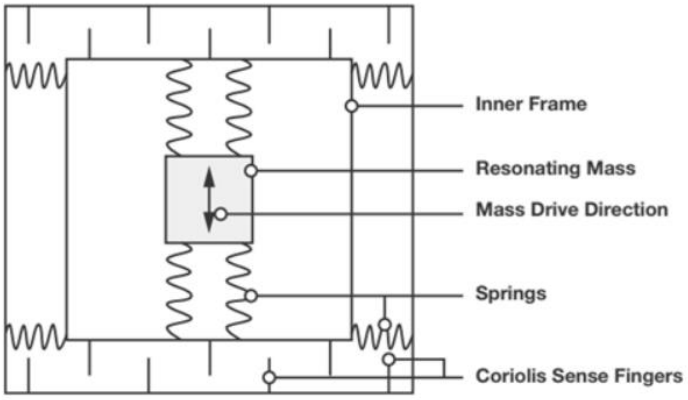

Figure 1: MEMS Gyroscope

2. MEMS Accelerometer

Accelerometer has a proof mass representing a spring mass damping system. The proof mass is placed between two plates with gaps between plates and mass. Sensor

movement displaces the proof mass causing a change in capacitance, which gives a measure of acceleration of proof mass depicting the acceleration of object holding the sensor. Figure 2 [3] illustrates a simplified structure of a MEMS Accelerometer.

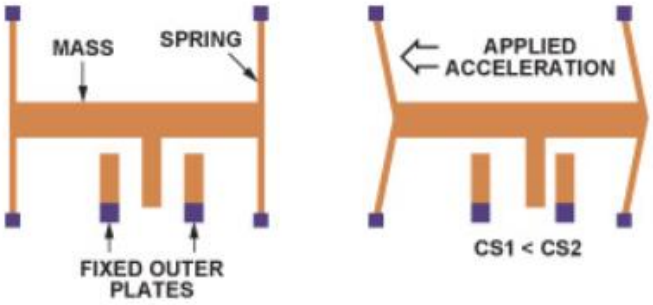

Figure 2: MEMS Accelerometer

3. MEMS Magnetometer

It measures earth magnetic field and any anomaly fields using hall effect or magneto resistive effect. The change in magnetic field redistributes the flow of electrons in a thin conductive plate thereby creating a voltage difference. Figure 3 Illustrates working of Hall effect.

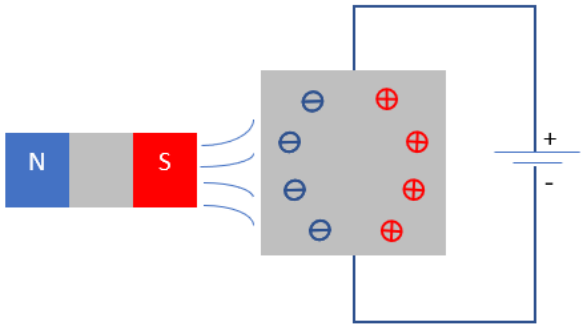

Figure 3: Hall effect Illustration

1.3 Review of Prior and Related Work

A review of prior and related work is organized in three subsections based on the general procedures of the indoor localization: 1) orientation and position estimation, 2) sensor fusion techniques.

1.3.1 Orientation and Position Estimation

Orientation estimation is the first step for indoor localization and can be obtained with different methods. For a VIP, navigation to a certain location is not possible through communication between brain and eyes. Cameras or visual sensors come next to eyes to capture surrounding information and can be used for orientation and position estimation of a VIP. Vision-based navigation for robots [4,5] have been proposed, however, a VIP movement is complex and unsteady compared to a rigid body of a robot. Also, for accuracy a very complex algorithm is required and must be based on artificial intelligence or machine learning, which are at its nascent stage. But few methods like edge detection and fingerprinting methods [6,7] can be used where a large database of building pictures is gathered and compared with current location. This method is highly inaccurate with picture comparison and takes up a huge database processing time. Other method would be to use magnetometers. Magnetic compass has long been used previously to navigate in a certain direction. Advancements in MEMS technology [8] have made these magnetometers very compact. Although these give approximate orientation, raw use of this technology is not recommended for a VIP in indoor orientation estimation as the magnetic field is influenced by the surrounding ferrous objects [9]. A good estimate of orientation can also be obtained from gyroscope readings as the angle rotated from the initial position is integrated [10].

Gyroscopes have long been used for flight and rocket navigation and are very bulky. MEMS gyroscopes are very compact and cheap but have accuracy issues as they suffer from drift if used for long time [11].

After orientation estimation, localization would only be complete with position estimation. Wi-fi is used everywhere which uses designated spectrum of radio frequencies to communicate with devices. Like satellites for GPS, routers arranged at different locations can be used to identify the user's position using triangulation method [12]. There are three ways to this method, Time of Arrival (Lateration method), Angle of arrival (Angulation method) and RSSI (radio signal strength indicator). The above-mentioned methods are accurate to 3-5m as they have multipath issues which leads to incorrect position. Like Wi-fi technology, Radio Frequency Identification (RFID) is another method which uses transmitter and receiver technique [13] with tags placed at different reference locations. A method proposes a smart floor with RFID tags transmitting unique ID's at all times to a portable terminal unit consisting RFID reader attached to VIP [14]. Similar use of RFID has been proposed with robot [15] and smartphones [16,17] as a portable unit. Limitations, however, include time and effort for reconfiguration. The accuracy of this method depends on the distance between each tag. Despite low accuracy, radio frequency method would be best for a normal person as he/she would use interpretation to reach the destination. However, for a VIP this might not be a best option. Like RFID tags Infrared LED's have been proposed in [18,19] which are placed strategically indoor. However, for efficient transmission of Infrared signal, the source must be directed towards the receiver, which would be impossible for a VIP. A method named Dristi [20] proposes OEM

ultrasonic pilots placed in a room, two beacons and wearable computer attached to the VIP. This method is accurate and proposes to be switchable between indoor and outdoor. However, the fact that the system being very bulky is not practically wearable by a VIP. Magnetic sensors are another method of obtaining a user's position. A magnetic sensor reads the surrounding magnetic field but gets distorted by surrounding objects. Magnetic maps can be generated by moving the sensor on the hallway of a building using these sensors and will be used as a reference map. When a VIP moves through the same hallway with sensor, a new map is generated and can be compared with reference map to obtain the position. However, as the navigation solely depends on the surrounding objects, any drastic change in surrounding results in change of magnetic map, which makes this method unreliable [21,22]. MEMS IMU generally include an accelerometer and gyroscope. Gyroscope has been discussed in earlier section and is used for orientation estimation. Accelerometers on the other hand, can be used for position estimation by double integration of accelerometer data. However, there are disadvantages as the accuracy is not recommended for navigation. Even a well calibrated IMU [23] tend to drift over long time usage due to double integration of accelerometer data to get the position of a user [24]. The accuracy can be resolved by a mounting the IMU on the foot of user. This method is called Zero Velocity Update (ZVU) and would have frequent stationary intervals for the IMU [25] to reduce the error. However, only high cost ($1000) IMU's proved to be accurate with ZVU method and low cost ($50) IMU's accuracy must be addressed.

1.3.2 Sensor Fusion Technique

From discussions in orientation and position estimation literatures, every sensor has its pros and cons and if used as a single sensor, the result will not be accurate. To overcome this accuracy issue, a technique called sensor fusion is implemented. This technique basically, combines results of all implemented sensors and give a better result than using a single sensor. There are sensor fusion algorithms which can be used like complimentary filter, Kalman filter, Extended Kalman filter, particle filter and some algorithms like AHRS and gradient decent specific for orientation estimation. Complimentary filter is basically a combination of high pass filter and low pass filter giving weightage for best of both. Kalman filter [26-29] and Extended Kalman filter uses a series of measurements observed over time containing statistical noise, inaccuracies and produces estimates of unknown variables that tend to be more accurate than those based on a single measurement alone. Particle filter is another filtering technique which uses Monte-Carlo method for estimation using random particles with gaussian noise. However, this method is useful to know a person's location but would not be able to guide a VIP [30].

1. Sensor Fusion for Orientation Estimation

There have been many researches on human motion analysis using Attitude and Heading Reference Systems (AHRS), which understands the orientation of limbs using IMU mounted on human body. Sensor data can be fused using complimentary [31,32], gradient decent and Kalman [33-35] for attitude estimation. However, Kalman does provide accuracy but is computationally complex [36-42]. AHRS Algorithms used by Mahony, which uses only accelerometer and gyroscope works on complimentary filter,

having both proportional and integral gains. Madgwick AHRS [43] uses magnetometer, gyroscope and accelerometer sensors with the use of use gradient decent method.

2. Sensor Fusion for Position Estimation

Wi-Fi can be used in combination with an IMU [44] mounted on human body or a magnetic map from magnetometer [45] for position estimation. However, Wi-fi needs additional infrastructure and maintenance. A monocular camera and an IMU has been used to complement each other using extended Kalman filter, where image processing technique like canny edge detection has been implemented [46]. However, image processing does take up time and depends on the optical conditions. Step detection is used widely to find the position of the user with an IMU mounted on foot. A double integration of acceleration for step length and heading information from gyroscope and magnetometer are clubbed using Kalman filter for position estimation [47,48]. Walking pattern is different for every individual and every limb in human body has specific acceleration. Placement of IMU on a human body must be chosen such that the drift can be corrected significantly. Other mounting methods include IMU attached to chest [49] and waist [50] for step detection and a particle filter is used to match position with floor map. A method has been implemented using magnetic coils arranged across the building generating magnetic field in combination to an IMU. However, like Wi-Fi, infrastructure is a problem [51,52]. IMU in smartphones have been used to generate magnetic map to aid inertial navigation by accelerometers [53,54]. This method of estimation using a smart phone are accurate than standalone IMU or magnetic map. However, foot mounted MEMS IMU has more advantages than a smartphone IMU. From literature study many ideas have been discussed like, Wi-Fi, RFID,

MEMS IMU, cameras, magnetic sensors and sensor fusion methods. However, multipath and interference issues with radio frequencies, drift issues with inertial sensors, computational restriction with cameras and change of magnetic map with surrounding objects motivate us to develop a method for VIP indoor localization. The fact that MEMS IMU's reduce error when mounted on user foot (ZVU method) can be used in a better way to get accurate localization. On other hand, magnetic map from geo magnetic sensors has a possibility to compliment an IMU.

1.4 Problem Description and Objectives

Inspired by the fact that birds utilize the geomagnetic field for homing and migration, magnetic distortion or anomalies by steel structures, electrical closets, metal doors or frames in a building can be used for indoor navigation of an VIP. Meanwhile, to minimize the localization uncertainty and eliminate the effects of the magnetic fluctuation on the estimation, inertial information is integrated using sensor fusion methods. This can be achieved by three objectives.

- The *first* objective is to estimate the orientation/position using inertial information. The inherently accumulative drift will be eliminated by using the characteristics of human walking.
- The *second* objective is to estimate the position with geomagnetic information for the VIPs. The orientation information will be involved to correct the deviation introduced by the orientation difference between the magnetic map and real-time data.

- The *third* objective is to fuse the inertial and geomagnetic information to obtain accurate, reliable and robust position estimation.

1.5 Outline and Organizations of Thesis

Thesis can be outlines into five chapters discussing every stage of the project and methodology. Chapter 2 explains the different segments of orientation estimation, DTW and sensor fusion algorithms for VIP indoor localization. Sensing system design required for the proposed algorithm is discussed in Chapter 3. Experimental demonstration and analysis of the proposed method is discussed in Chapter 4 followed by conclusion and future work in Chapter 5.

Chapter 2. Indoor Localization Using Inertial and Geomagnetic Information

To successfully guide the VIPs indoor with low cost and high efficiency and accuracy, a new indoor localization method is developed using two types of naturally-generated physical information, inertial and geomagnetic information.

Inertial sensors such as accelerometers and gyroscopes are capable of directly measuring the acceleration and angular velocity. Mathematically, the location and orientation can be estimated by doing the integration. However, the measurement errors will be amplified/accumulated by the integration operation, which will contaminate the estimation results. Inspired by the fact that birds utilize the geomagnetic field for homing and migration, magnetic distortion or anomalies by steel structures, electrical closets, metal doors or frames in a building can be used for indoor navigation of a VIP. To minimize the localization uncertainty and eliminate the effects of the passive physical parameter fluctuation on the estimation, new sensor fusion algorithms are developed to provide more accurate indoor location estimation after individual analysis of indoor localization using inertial and geomagnetic information.

In order to conduct indoor position tracking, several coordinate frames need to be introduced at first. To simplify this problem, we assume the earth is stationary and the earth frame is an inertial frame as shown in Figure 4 [55]

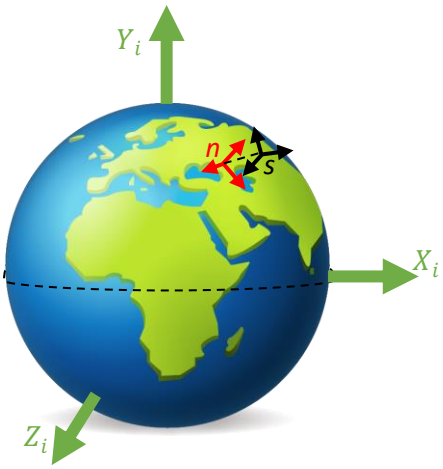

Figure 4: Co-ordinate Frame Representation

- *Sensor frame* (*s*) is the coordinate frame of inertial sensors with its origin located at the center of sensors. All sensor readings are with respect to this frame.
- *Navigation frame* (*n*) is a local coordinate frame that is defined as stationary with respect to the earth. The results of position tracking are the estimation of the location and orientation of the sensor frame with respect to the navigation frame.
- *Inertial/earth frame* (*i*) is a stationary frame with the origin located at the center of the earth. The inertial sensors measure the linear acceleration and angular velocity with respect to the inertial frame.

Since there is no relative motion between the navigation frame and inertial frame, inertial sensors are assumed to measure the linear acceleration / angular velocity with respect to navigation frame.

2.1 Orientation Representation

Since several frames are utilized to perform the indoor localization as introduced above. The transformation and orientation representation between all those frames are critical and basis for the localization algorithms. Three types of orientation representation are introduced in this section.

1. Euler Angle Representation

Euler angles are indicated by pitch, roll and yaw, which follows a sequence of rotations *X-Y-X*, *X-Z-X*, *Y-X-Y*, *Y-Z-Y*, *Z-X-Z* and *Z-Y-Z* with the first and third rotation about same axis. Tait-Bryan conventions follows *X-Y-Z*, *X-Z-Y*, *Y-X-Z*, *Y-Z-X*, *Z-X-Y* and *Z-Y-X*. Let φ, θ, ψ be pitch, roll and yaw respectively. A rotation [**R**] can be defined by each axis rotation from Eq.(1a,b,c)

$$[\mathbf{R}] = Z(\psi)Y(\theta)X(\varphi) \tag{1a}$$

$$[\mathbf{R}_X] = \begin{bmatrix} 1 & 0 & 0 \\ 0 & \cos\varphi & -\sin\varphi \\ 0 & \sin\varphi & \cos\varphi \end{bmatrix} \quad [\mathbf{R}_Y] = \begin{bmatrix} \cos\theta & 0 & \sin\theta \\ 0 & 1 & 0 \\ -\sin\theta & 0 & \cos\theta \end{bmatrix}$$

$$[\mathbf{R}_Z] = \begin{bmatrix} \cos\psi & -\sin\psi & 0 \\ \sin\psi & \cos\psi & 0 \\ 0 & 0 & 1 \end{bmatrix} \tag{1b}$$

$$[\mathbf{R}] = \begin{bmatrix} \cos\theta\cos\psi & -\cos\varphi\sin\psi + \sin\varphi\sin\theta\cos\psi & \sin\varphi\sin\psi + \cos\varphi\sin\theta\cos\psi \\ \cos\theta\sin\psi & \cos\varphi\cos\psi + \sin\varphi\sin\theta\sin\psi & -\sin\varphi\cos\psi + \cos\varphi\sin\theta\sin\psi \\ -\sin\theta & \sin\varphi\cos\theta & \cos\varphi\cos\theta \end{bmatrix} \tag{1c}$$

However, due to the usage of trigonometry functions in the multiplication of matrices, Euler angles suffer with gimble lock, where one degree of freedom is lost. Gimble lock can be addressed by cumulative matrix transformation method. However, it is computationally expensive.

2. Equivalent Axis-Angle Representation

Axis-Angle is another representation shown in Figure 5, which defines any orientation as a rotation of a vector, $\hat{a} = (a_x, a_y, a_z)^T$, about an axis, $\hat{e}$, of an angle, α. Rotation, [**R**], can be represented from Eq.2. However, Axis-Angle is also computationally expensive.

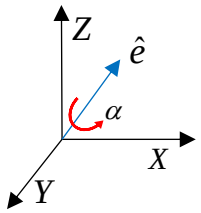

Figure 5: Angle-Axis Representation

$$[\mathbf{R}] = \begin{bmatrix} \cos\alpha + a_x^2(1-\cos\theta) & a_x a_y(1-\cos\alpha) - a_z\sin\alpha & a_y\sin\alpha + a_x a_z(1-\cos\alpha) \\ a_z\sin\alpha + a_x a_y(1-\cos\alpha) & \cos\alpha + a_y^2(1-\cos\theta) & -a_x\sin\alpha + a_y a_z(1-\cos\alpha) \\ -a_y\sin\alpha + a_x a_z(1-\cos\alpha) & a_x\sin\alpha + a_y a_z(1-\cos\alpha) & \cos\alpha + a_z^2(1-\cos\theta) \end{bmatrix} \quad (2)$$

3. Quaternion Representation

Like Axis-Angle, Quaternions representation also states that any rotation or sequence of rotation of a moving coordinate *B* about a fixed coordinate *A* can also be interpreted as a single rotation by an angle α about a fixed axis (called Euler axis), which is represented with a unit vector $\vec{\mathbf{u}} = \begin{bmatrix} u_x & u_y & u_z \end{bmatrix}^T$. Thereby, a combination of a unit

vector representing the axis and a scalar angle can uniquely determine a 3D rotation or the orientation of coordinate *B* relative to coordinate *A*. A number system, quaternions, consisting of four numbers are introduced to mathematically represent this quaternion rotation or orientation as below

$$\mathbf{q}^{BA} = \begin{bmatrix} q_1 & q_2 & q_3 & q_4 \end{bmatrix} = \begin{bmatrix} \cos\alpha/2 & -u_x \sin\alpha/2 & -u_y \sin\alpha/2 & -u_z \sin\alpha/2 \end{bmatrix} \quad \text{(3a, b)}$$

The inverse (denoted by subscript $^{-1}$) or conjugate (denoted by subscript *) of the quaternion rotation are introduced to represent the opposite rotation or swapped relative orientation, which is mathematically expressed in Eq. (4).

$$\left(\mathbf{q}^{BA}\right)^{-1} = \left(\mathbf{q}^{BA}\right)^{*} = \begin{bmatrix} q_1 & -q_2 & -q_3 & -q_4 \end{bmatrix} = \mathbf{q}^{AB} \quad \text{(4a, b)}$$

where $\mathbf{q}^{AB}$ represents the orientation of coordinate *A* with respect coordinate *B*.

To represent a sequential orientation and coordinate transformation, the Hamilton product (denoted by $\otimes$) of the quaternion is introduced in Eq. (5). This product is not commutative, which is expressed as $\mathbf{m} \otimes \mathbf{n} \neq \mathbf{n} \otimes \mathbf{m}$.

$$\begin{aligned} \mathbf{m} \otimes \mathbf{n} &= \begin{bmatrix} m_1 & m_2 & m_3 & m_4 \end{bmatrix} \otimes \begin{bmatrix} n_1 & n_2 & n_3 & n_4 \end{bmatrix} \\ &= \begin{bmatrix} m_1 n_1 - m_2 n_2 - m_3 n_3 - m_4 n_4 \\ m_1 n_2 + m_2 n_1 + m_3 n_4 - m_4 n_3 \\ m_1 n_3 - m_2 n_4 + m_3 n_1 + m_4 n_2 \\ m_1 n_4 + m_2 n_3 - m_3 n_2 + m_4 n_1 \end{bmatrix}^{\mathrm{T}} \end{aligned} \quad (5)$$

Assume another coordinate *C* is introduced and its orientation $\mathbf{q}^{CB}$ with respect to coordinate *B* is given. The orientation of *C* relative to *A* is represented with the quaternion product in Eq. (6).

$$\mathbf{q}^{CA} = \mathbf{q}^{CB} \otimes \mathbf{q}^{BA} \tag{6}$$

Assume $\mathbf{u}^A$ is a vector described in coordinate *A*. A 0(zero) is inserted to this vector to make it a row vector containing 4 elements. Given the relative orientation of coordinate B represented with $\mathbf{q}^{AB}$, the same vector described in coordination B is expressed in Eq. (7).

$$\mathbf{u}^B = \mathbf{q}^{BA} \otimes \mathbf{u}^A \otimes \left(\mathbf{q}^{BA}\right)^* \tag{7}$$

It can also be represented in a rotation matrix form.

$$\mathbf{u}^B = \mathbf{u}^A \left[\mathbf{R}_A^B\right] \tag{8a, b}$$

$$\text{where } \left[\mathbf{R}_A^B\right] = \begin{bmatrix} 2q_1^2 + 2q_2^2 - 1 & 2\left(q_2 q_3 + q_1 q_4\right) & 2\left(q_2 q_4 - q_1 q_3\right) \\ 2\left(q_2 q_3 - q_1 q_4\right) & 2q_1^2 + 2q_3^2 - 1 & 2\left(q_3 q_4 + q_1 q_2\right) \\ 2\left(q_2 q_4 + q_1 q_3\right) & 2\left(q_3 q_4 - q_1 q_2\right) & q_1^2 + q_4^2 - 1 \end{bmatrix}$$

2.2 Orientation Estimation using IMU

With the angular velocity $\boldsymbol{\omega}_{ns}^s$ represented in the quaternion form shown in Eq. (9a), the time rate of the orientation of the navigation frame relative to the sensor frame expressed with quaternion can be calculated using Eq. (9b).

$$\hat{\boldsymbol{\omega}}_{ns}^s = \begin{bmatrix} 0 & \hat{\omega}_x & \hat{\omega}_y & \hat{\omega}_z \end{bmatrix}, \dot{\mathbf{q}}^{ns} = \frac{1}{2}\mathbf{q}^{ns} \otimes \hat{\boldsymbol{\omega}}_{ns}^s \tag{9a, b}$$

By numerically integrating the quaternion derivative $\dot{\mathbf{q}}^{ns}$, the orientation of the navigation frame relative to the sensor frame $\mathbf{q}_t^{ns}$ can be calculated with Eq. (10b).

$$\dot{\mathbf{q}}_t^{ns} = \frac{1}{2}\mathbf{q}_{est,t-1}^{ns} \otimes \boldsymbol{\omega}_{ns,t}^s, \ \mathbf{q}_{est,t}^{ns} = \mathbf{q}_{est,t-1}^{ns} + \dot{\mathbf{q}}_t^{ns}\Delta t \tag{10a, b}$$

where, Δt is the time interval, $\mathbf{q}_{est,t-1}^{ns}$ is the previous orientation estimation.

2.2.1 Data Pre-processing

Any error in orientation estimation of the foot in the navigation frame results in position error. In attitude estimation, accelerometer data is used in combination with gyroscope for correcting the pitch and roll during stationary and motion periods. Stationary accelerations would only include gravity component; however, motion period would include gravity component as well as any external accelerations. The latter is sufficiently higher to contaminate the orientation. Hence, a low pass filtering of accelerometer measurement $\hat{\mathbf{a}}_{ns}^{s}$ is required to ensure removal of high frequency components which mostly contributed by the motion and retain gravity component for orientation correction, giving out $\hat{\mathbf{a}}_{ns,t}^{s,F}$ as low pass filtered data.

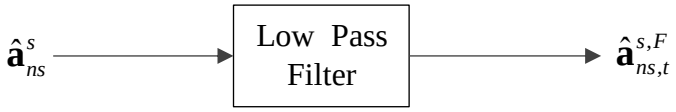

Figure 6: Low Pass Filtering of Accelerometer Data

2.2.2 Orientation Estimation

Given the orientation represented with $\mathbf{q}^{ns} = \begin{bmatrix} q_1 & q_2 & q_3 & q_4 \end{bmatrix}$, the gravitational acceleration with respect to the sensor frame $\mathbf{a}_{ns}^{s}$ can be calculated with Eq. (11).

$$\mathbf{a}_{ns}^{s} = \left(\mathbf{q}^{ns}\right)^{*} \otimes \mathbf{a}_{ns}^{n} \otimes \mathbf{q}^{ns} = \begin{bmatrix} 2\left(q_2 q_4 - q_1 q_3\right) \\ 2\left(q_1 q_2 + q_3 q_4\right) \\ 2\left(0.5 - q_2^2 - q_3^2\right) \end{bmatrix} \quad \text{(11a, b)}$$

Where, $\mathbf{a}_{ns}^{n} = \begin{bmatrix} 0 & 0 & 0 & 1 \end{bmatrix}$ is the gravitational acceleration with respect to the inertial frame (navigation frame).

Due to the accumulated error in the orientation estimation $\mathbf{q}_{est,t-1}^{ns}$, there is a deviation between $\mathbf{a}_{ns,t}^{s}$ and $\hat{\mathbf{a}}_{ns,t}^{s,F}$ (the measurements of the accelerometer), which is expressed in Eq. (12a) and Figure 7. The angular velocity is updated with the deviation as $\mathbf{e}_t^a$ and Eq. (12b).

$$\mathbf{e}_t^a = \mathbf{a}_{ns,t}^{s} \times \hat{\mathbf{a}}_{ns,t}^{s,F}, \quad \boldsymbol{\omega}_{ns,t}^{s} = \hat{\boldsymbol{\omega}}_{ns,t}^{s} + K_P^a \mathbf{e}_t^a \quad \text{(12a, b)}$$

where $\hat{\boldsymbol{\omega}}_{ns,t}^{s}$ is the measurement of the gyroscope at time t, K_P^a is a constant, which is similar to the gain of Proportional controller. With the corrected angular velocity obtained from Eq. (12b), the orientation can be estimated with Eq. (10). Figure 8 illustrates the overall algorithm for orientation estimation.

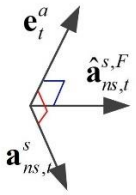

Figure 7: Deviation calculation

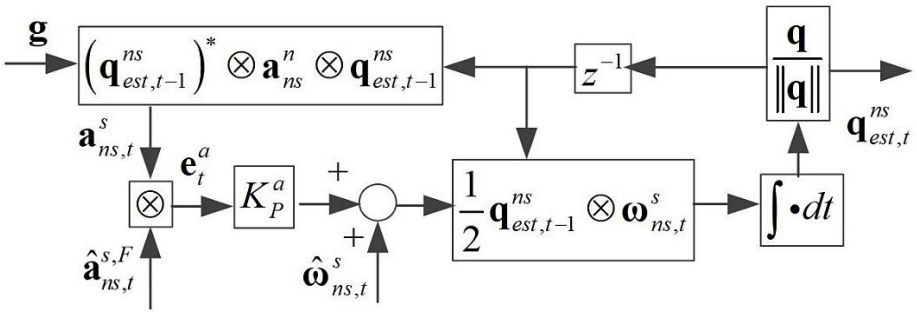

Figure 8: Flowchart illustrating orientation estimation

2.3 Position Estimation using IMU

As mentioned above, the position can be estimated by double integration, which consequently introduces accumulative errors or drifts. By analyzing the gait phase of human (stance, heel-off, swing, and heel-strike), a method to correct the accelerometer drift is developed.

2.3.1 Stationary Phase Detection

The drift issues caused by long time usage of IMU can be reduced with the stationary phase detection method. This method requires the VIP to mount the IMU to one of his/her foot making use of stationary and motion intervals of walking foot. However, before stationary phase detection, accelerometer data is to be low-pass filtered to eliminate any existing noise. The filtered three acceleration components are close to zero for a stationary foot and non- zero for a walking foot. A magnitude of three acceleration components at each instant would help identify stationary and motion intervals for below and above threshold value respectively as shown in Figure 9

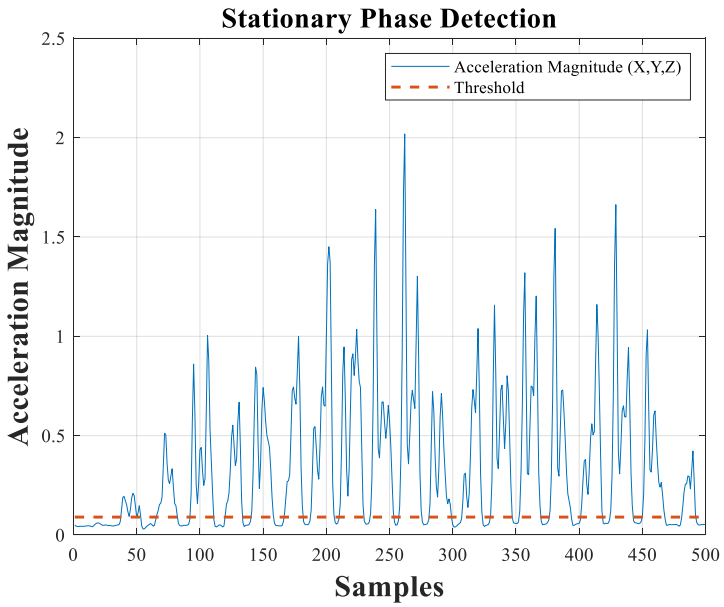

Figure 9: Illustration of Stationary Detection

2.3.2 Zero Velocity Update and Drift Correction

After threshold identification from stationary detection method, the velocity of the stationary phases (the rest three phases) should be approximately zero, which can be used for velocity and accelerometer drift correction represented with Eq.13. The acceleration measurements need to be converted from sensor frame ($\hat{\mathbf{a}}_{ns}^{s}$) to navigation frame ($\hat{\mathbf{a}}_{ns}^{n}$) with Eq.7 before correction and integration. Figure 10 shows the integrated velocity and displacement of one period motion (1 meter) before and after drift correction with non-zero final velocity in Figure 10(a) and zero final velocity in Figure 10(b).

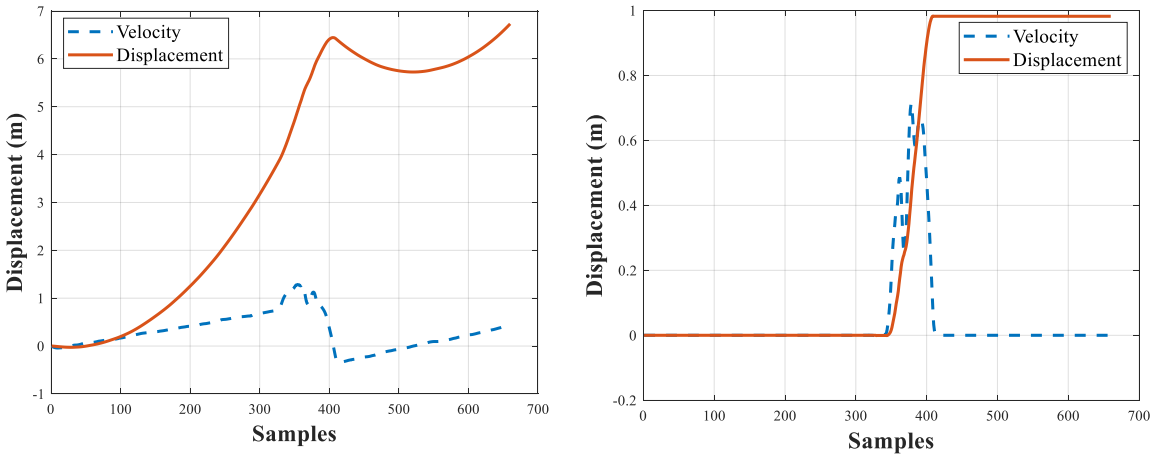

(a) Original Data (a) Corrected Data

Figure 10: Illustration of Velocity drift correction

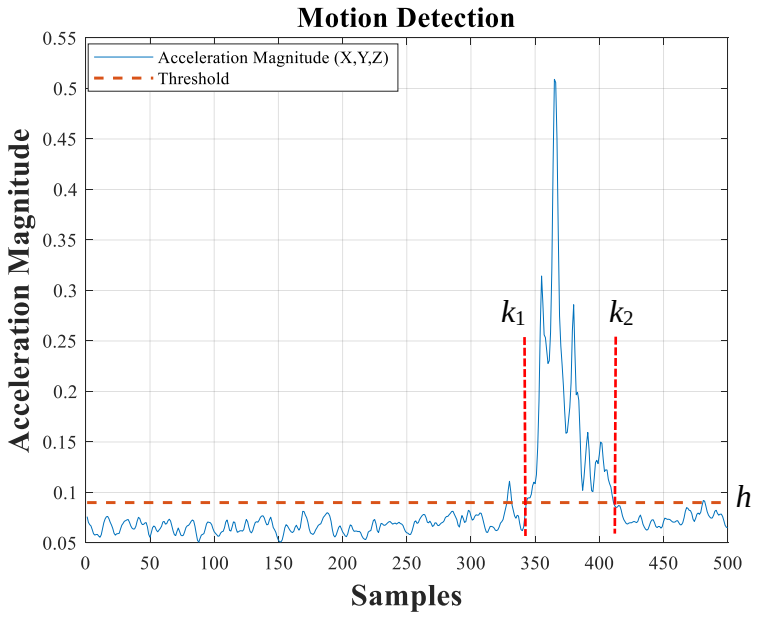

Figure 11: Illustration of motion detection

$$\hat{\mathbf{v}}_{ns}^{n}(t) = \hat{\mathbf{v}}_{ns}^{n}(t-1) + \hat{\mathbf{a}}_{ns}^{n}(t)\Delta t, \tag{13a}$$

$$\mathbf{v}_{ns}^{n}(t)=\begin{cases}0 & t\le k_1\\ \hat{\mathbf{v}}_{ns}^{n}(t)-\dfrac{\hat{\mathbf{v}}_{ns}^{n}(k_2)}{(k_2-k_1)}(t-k_1) & k_1<t\le k_2\\ 0 & t>k_2\end{cases}$$

$$\mathbf{a}_{ns}^{n}(t)=\begin{cases}0 & t\le k_1\\ \hat{\mathbf{a}}_{ns}^{n}(t)-\dfrac{\hat{\mathbf{v}}_{ns}^{n}(k_2)}{(k_2-k_1)T} & k_1<t\le k_2\\ 0 & t>k_2\end{cases} \tag{13b}$$

$$\mathbf{p}^{n}(t)=\mathbf{p}^{n}(t-1)+\mathbf{v}_{ns}^{n}(t)\Delta t+\frac{1}{2}\mathbf{a}_{ns}^{n}(t)\Delta t^{2} \tag{14}$$

where Δt is the sampling period of the inertial sensor, k_1 and k_2 are the starting and ending points of the motion for this period (swing phase), which can be automatically detected based on the acceleration measurement. The acceleration will be within a user-defined threshold *h* illustrated by two red dash lines in Figure 11 if the foot or sensor does not move (stationary phases). The position can be calculated with corrected velocity $\mathbf{v}_{ns}^{n}$ and acceleration $\mathbf{a}_{ns}^{n}$ as shown in Eq. (14).

2.4 Position Estimation using MTS

By observing the phenomenon that the magnetic anomalies introduced by the magnetic objects indoor have different and unique features and characters at different locations, the distorted geomagnetic field has the potential to be used as an approach to offer location information, which is a good supplement for indoor localization using inertial information.

2.4.1 Magnetic Flux Density and Gradient

Generally speaking, the measurements of the geomagnetic field **T** consists of three components, geomagnetic field $\mathbf{B}_E$, magnetic fields generated by man-made magnetic objects **B** and unmodeled magnetic field $\mathbf{B}_U$ as illustrated in Eq. (15). Although indoor location information can be indicated by **B**, **B** is relatively small and cannot be directly measured with the existence of B_E. Magnetic tensor [**G**], which is a 3×3 symmetric and trackless matrix with the expressions shown in Eq. (16), is introduced to extract the information of the magnetic anomalies due to $\left|\nabla \mathbf{B}_E\right| \approx 0.02\left(\mathrm{nT/m}\right)$ and $\nabla \mathbf{T} \approx \nabla \mathbf{B}$ with ignorable $\mathbf{B}_U$.

$$\mathbf{T} = \mathbf{B} + \mathbf{B}_E + \mathbf{B}_U \tag{15}$$

$$\left[\mathbf{G}\right] = \frac{\partial \mathbf{B}}{\partial \mathbf{R}} = \begin{bmatrix} \partial_x B_x & \partial_y B_x & \partial_z B_x \\ \partial_x B_y & \partial_y B_y & \partial_z B_y \\ \partial_x B_z & \partial_y B_z & \partial_z B_z \end{bmatrix} \tag{16a}$$

$$\left[\mathbf{G}\right] = \left[\mathbf{G}\right]^{\mathrm{T}} \text{ and } \partial_x B_x + \partial_y B_y + \partial_z B_z = 0 \tag{16b, c}$$

2.4.2 DTW Algorithm

A reference magnetic map, consisting of spatial magnetic information can be built using **B** and **G.** Intuitively, by matching the real-time measured magnetic information with a reference magnetic map, the location will be estimated. However, the walking speed is time-varying, which introduces some difficulties. Based on the traditional Dynamic Time Warping (DTW) method, a well-known technique to find an optimal alignment between two given time-dependent sequences, an improved subsequence DTW with the characteristics of computing time and space efficiency is introduced to conduct indoor

localization. We first define classical DTW, which is the basis, followed by the improved subsequence DTW.

1. Classical DTW

This method compares two different time series for a match between all the elements using a low-cost measure also known as local distance measure validating the extent of match between elements. Typically, a low-cost would mean a good match as an optimal match usually runs along all the low-cost measures. A cost matrix, $C \in \mathbb{R}^{N \times M}$ defined by $C(n,m) := c(x_n, y_m)$, can be obtained from all the elements of sequences defined as $X = \{x_1, x_2, ..., x_N\}$ where $n = [1:N]$, $N \in \mathbb{N}$ and $Y = \{y_1, y_2, ..., y_M\}$ where $m = [1:M]$, $M \in \mathbb{N}$. Alignment match referred to as $p = \{p_1, p_2, ..., p_L\}$, with $p_l = (n_l, m_l) \in [1:N] \times [1:M]$ for $l \in [1:L]$ is obtained satisfying three conditions.

(i) Boundary Condition: $p_1 = (1,1)$ and $p_l = (N, M)$

(ii) Monotonicity Condition: $n_1 < n_2 < n_3 ..... < n_L$ and $m_1 < m_2 < m_3 ..... < m_L$

(iii) Step-size Condition: $p_{l+1} - p_l \in \{(1,0),(0,1),(1,1)\}$ for $l \in [1:L-1]$

The total cost matrix is defined by Eq. (17)

$$c_p(X,Y) := \sum_{l=1}^{L} c(x_{n_l}, y_{m_l}) \tag{17}$$

However, many alignment paths/matches are obtained from $c_p(X,Y)$, requiring many exponential computations. An accumulated cost matrix, $D(n,m)$, can be defined to identify an optimal low-cost alignment satisfying Eq. (18d) and setting $D(n,0) := \infty$ for $n \in [1:N]$, $D(0,m) := \infty$ for $m \in [1:M]$ and $D(0,0) := 0$.

$$D(n,m) \coloneqq \text{DTW}\ (X(1:n), Y(1:m)) \tag{18a}$$

$$D(n,1) = \sum_{k=1}^{n} c(x_k, y_1)\ \ for\ n \in [1:N] \tag{18b}$$

$$D(1,m) = \sum_{k=1}^{m} c(x_1, y_k)\ \ for\ m \in [1:M] \tag{18c}$$

$$D(n,m) = \min\{D(n-1,m-1), D(n-1,m), D(n,m-1)\} + c(x_n, y_m) \quad for\ 1 < n \le N\ and\ 1 < m \le M \tag{18d}$$

However, classical DTW has a boundary condition enforcing match for the whole time series i.e., first and last element.

2. Subsequence DTW

This method is an improvisation to classical DTW for a case where one-time sequence is part of another time sequence making it suitable for magnetic map matching as the measurement map is significantly smaller than reference map, intuitively making it a part of reference map. For $X = \{x_1, x_2, ..., x_N\}$ and $Y = \{y_1, y_2, ..., y_M\}$, M is significantly larger than *N*. $Y(a^* : b^*) \coloneqq (y_{a^*}, y_{a^*+1}, ..., y_{b^*})$ with $1 \le a^* \le b^* \le M$

$$(a^*, b^*) \coloneqq \underset{(a,b):1\le a\le b\le M}{\arg\min} \left(DTW\left(X, Y\left(a:b\right)\right)\right) \tag{19}$$

A modification to accumulated cost matrix by defining Eq.20 and setting $D(n,0) \coloneqq \infty$ for $n \in [0:N]$, $D(0,m) \coloneqq 0$ for $m \in [1:M]$.

$$D(n,1) = \sum_{k=1}^{n} c(x_k, y_1)\ \ for\ n \in [1:N] \tag{20a}$$

$$D(1,m) = c(x_1, y_k)\ \ for\ m \in [1:M] \tag{20b}$$

The index b^* can be defined as Eq. (21). Figure 12 shows comparison of two sequences

$$b^* := \arg\min_{b \in [1:M]} D(N, b) \tag{21}$$

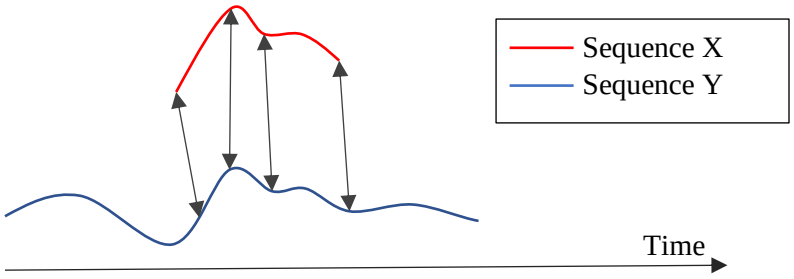

Figure 12: Illustration of subsequent DTW

In order to clearly and graphically illustrate the method, only one component of **T** is used to conduct the matching as illustrated in Figure 13. The real-time measured data and magnetic map are represented with red and blue curves respectively. The matching is conducted to find the best fit within the search window defined with the previously estimated location using the measured data in the sample window. The spatial information attached to the best fit within the search window indicates the estimated indoor location.

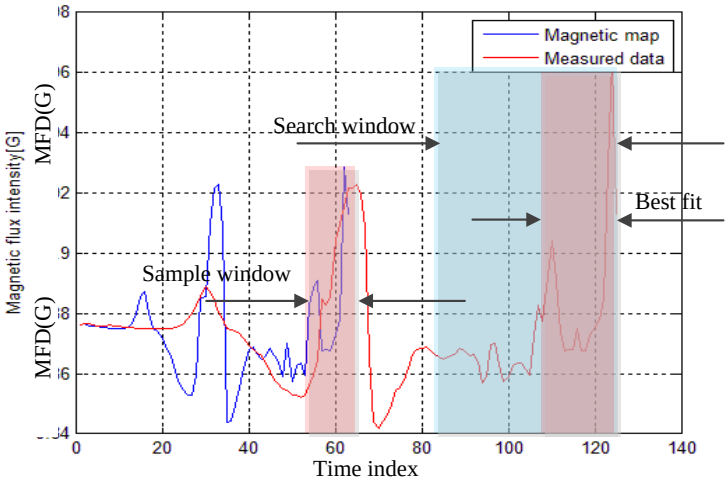

Figure 13: Illustration of improved subsequence DTW

2.5 Sensor Fusion Using Kalman Filter

Kalman Filter is introduced to fuse data from multiple sensors for a better estimation. Figure 14 [56] summarizes all the mathematical equations that the Kalman filter utilizes to estimate the system state. The Kalman filter goes in a loop or a cycle that consists of two steps: Time update and measurement update.

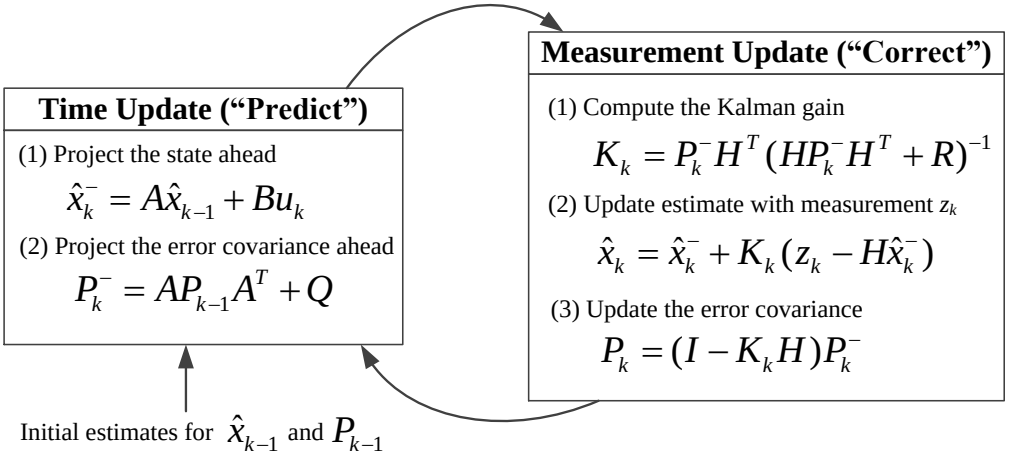

Figure 14: Schematics of Kalman filter

In Figure 14, $\hat{x}_k^-$ and $\hat{x}_k$ are *prior* and *posterior* estimates of the system state respectively. P_k is the co-variance matrix, which changes during both steps. A is the dynamics matrix, Q is the process noise co-variance matrix, B is a control matric and u_k is a control input. H is the measuring matrix, R is measurement noise covariance matrix, z_k is the measurement and K_k is dynamic Kalman gain.

2.5.1 Yaw Correction

Generally speaking, as the measurement of the gravitational acceleration can only be used for pitch and Roll correction, geomagnetic information is introduced to correct the heading. However, the existence of the magnetic anomalies will contaminate the geomagnetic field, resulting in a contaminated heading estimation. A Low pass filtering of the MFD components would solve this issue by eliminating any existing magnetic anomalies, VIP walking frequencies and any noise to some extent from the measurements which can be used to get the yaw angle as given by Eq. (23).

$$\mathbf{B} = \begin{bmatrix} B_X & B_Y & B_Z \end{bmatrix}^T \tag{22}$$

Figure 15: Magnetic Data Filtering

$$\psi^{geo} = \arctan(B_Y^{LP}, B_X^{LP}) \tag{23}$$

Euler angles are obtained using quaternion obtained from Mahony algorithm. Quaternion to rotation matric is represented as [**R**] from Eq. (8) and Euler angles from [**R**] are represented as Eq. (24a,b,c).

$$\varphi^{quat} = \arctan(R_{32}, R_{33}) \tag{24a}$$

$$\theta^{quat} = -\arctan(R_{31}, \sqrt{(1-R_{31}^2)}\ ) \tag{24b}$$

$$\psi^{quat} = \arctan(R_{21}, R_{11}) \tag{24c}$$

where, $\varphi^{quat}, \theta^{quat}, \psi^{quat}$ are Pitch, Roll and Yaw angles respectively. A better estimate of yaw angle is obtained from Kalman filter by fusing gyroscope and geomagnetic estimations with parameters as listed in Table 1 Where, ψ_t $\dot{\psi}_t^b$ $\dot{\psi}_t^{quat}$ are yaw angle, yaw angular rate bias and angular rate, obtained from *t* and *t*-1 instances of ψ^{quat} , respectively. The prediction step and update step for Kalman angle estimation is represented in Eq. (25) and Eq.26 respectively.

Table 1: Kalman System State Estimates for Yaw Correction

System State: $\hat{\mathbf{x}}_t = \begin{bmatrix} \psi_t & \dot{\psi}_t^b \end{bmatrix}^{\mathrm{T}}$	**Control Input:** $u_t = \dot{\psi}_t^{quat}$	**Measurement Input** $z_t = \psi_t^{geo}$
Matrix Coefficients: $[\mathbf{A}] = \begin{bmatrix} 1 & -\Delta t \\ 0 & 1 \end{bmatrix} [\mathbf{B}] = \begin{bmatrix} \Delta t \\ 0 \end{bmatrix} [\mathbf{H}] = [1 \quad 0]$		

$$\begin{bmatrix} \psi_k^- \\ \dot{\psi}_k^{b-} \end{bmatrix} = \begin{bmatrix} 1 & -\Delta t \\ 0 & 1 \end{bmatrix} \begin{bmatrix} \psi_{k-1} \\ \dot{\psi}_{k-1}^b \end{bmatrix} + \begin{bmatrix} \Delta t \\ 0 \end{bmatrix} \begin{bmatrix} \dot{\psi}_k^{quat} \end{bmatrix} \tag{25a}$$

$$\begin{bmatrix} \psi_k^- \\ \dot{\psi}_k^{b-} \end{bmatrix} = \begin{bmatrix} \psi_{k-1} + \Delta t \dot{\psi}_k^{quat} - \Delta t \dot{\psi}_{k-1}^b \\ \dot{\psi}_{k-1}^b \end{bmatrix} \tag{25b}$$

$$\begin{bmatrix} \psi_k \\ \dot{\psi}_k^b \end{bmatrix} = \begin{bmatrix} \psi_k^- \\ \dot{\psi}_k^{b-} \end{bmatrix} + \begin{bmatrix} K_1 \\ K_2 \end{bmatrix} \left[\psi^{geo} - [1 \quad 0] \begin{bmatrix} \psi_k^- \\ \dot{\psi}_k^{b-} \end{bmatrix} \right] \tag{26}$$

The updated yaw is used to estimate yaw angular rate error in sensor frame. Previously defined orientation estimation algorithm can be modified as shown in Figure 16.

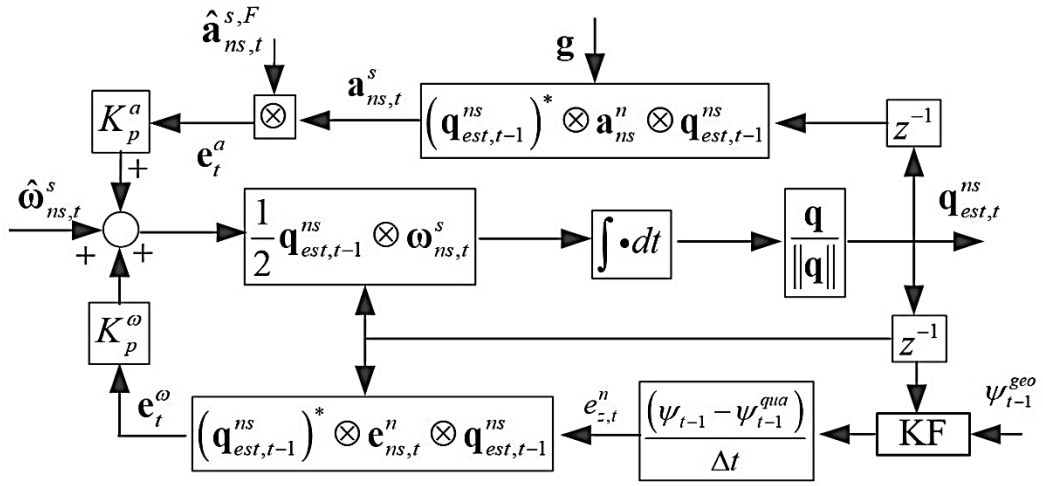

Figure 16: Modified Orientation Estimation Algorithm

However, even a low pass filtered MTS data is not good enough for heading estimation. Observing the phenomenon that the magnetic anomalies decrease rapidly with the increase of the distance, the magnetic spatial gradient (tensor) [**G**] can be utilized as an indicator to determine the existence of large magnetic anomalies. The geomagnetic information will be utilized only when a parameter *S*, which is the square root of the trace function of ([**G**][**G**]^{T}) as expressed in Eq. (27), is smaller than the preset threshold.

$$S = \sqrt{\text{trace}\left([\mathbf{G}][\mathbf{G}]^{T}\right)} \tag{27}$$

Figure 17 illustrates the effectiveness of *S* as an indicator to integrate the geo-information for yaw angle estimation. The estimation of yaw angle deviates from the true value when the calculated *S* is above the predefined threshold.

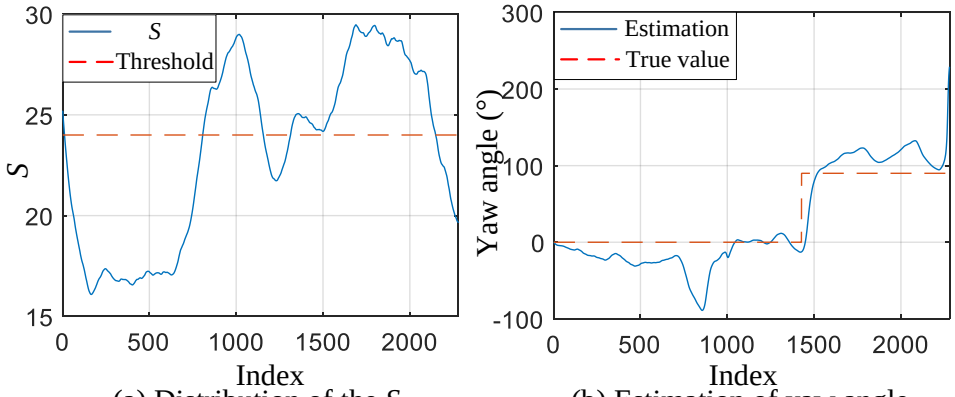

(a) Distribution of the *S* (b) Estimation of yaw angle

Figure 17: Geo-magnetic Gradient Threshold identification

2.5.2 Magnetic Map Correction

The characteristics of the magnetic information used to match the magnetic map are orientation-sensitive, which will lead to mismatch if the magnetic tensor sensor (MTS) orientation is not the same when acquiring data for matching and magnetic maps. Thereby, the estimated orientation will be introduced to correct the magnetic characteristics before conducting indoor localization using magnetic information. Besides the magnetic information, the sensor orientation when acquiring data for the magnetic map needs to be integrated into the map file. Assume $\mathbf{q}_t^{sn}$ and $\mathbf{q}_t^{\bar{s}n}$ represent the orientation of the MTS when acquiring data for matching and magnetic map respectively, the quaternion representation of the rotation from the matching orientation to map orientation $\mathbf{q}_t^{\bar{s}s}$ is expressed with Eq. (28a). The MFD and magnetic tensor will be corrected with Eq. (29) before conducting localization, where $\left[\mathbf{R}_s^{\bar{s}}\right]$ is the corresponding rotation matrix of $\mathbf{q}_t^{\bar{s}s}$; $\mathbf{B}_t^s$ and $\mathbf{B}_t^{\bar{s}}$ are the measured and corrected geo-MFD respectively; $\left[\mathbf{G}^s\right]$ and $\left[\mathbf{G}^{\bar{s}}\right]$ are measured and corrected magnetic tensor.

Figure 18 illustrates the process of the magnetic field correction for the MFD given the orientation deviation, where only yaw angle deviation is considered. Given the yaw angle deviation illustrated in Figure 18(b), the raw MFD data represented in Figure 18(c) is not similar to the magnetic map shown in Figure 18(a), which will lead to matching failure. By applying the magnetic field correction with Eq. (29a), the raw MFD data is corrected and manifested in Figure 18(d), which is similar to the magnetic map.

$$\mathbf{q}_t^{\bar{s}s} = \mathbf{q}_t^{\bar{s}n} \otimes \mathbf{q}_t^{ns}, \text{ where } \mathbf{q}_t^{ns} = \left(\mathbf{q}_t^{sn}\right)^* \tag{28a, b}$$

$$\mathbf{B}_t^{\bar{s}} = \mathbf{q}_t^{\bar{s}s} \otimes \mathbf{B}_t^{s} \otimes \left(\mathbf{q}_t^{\bar{s}s}\right)^*, \left[\mathbf{G}^{\bar{s}}\right] = \left[\mathbf{R}_s^{\bar{s}}\right]\left[\mathbf{G}^{s}\right] \tag{29a, b}$$

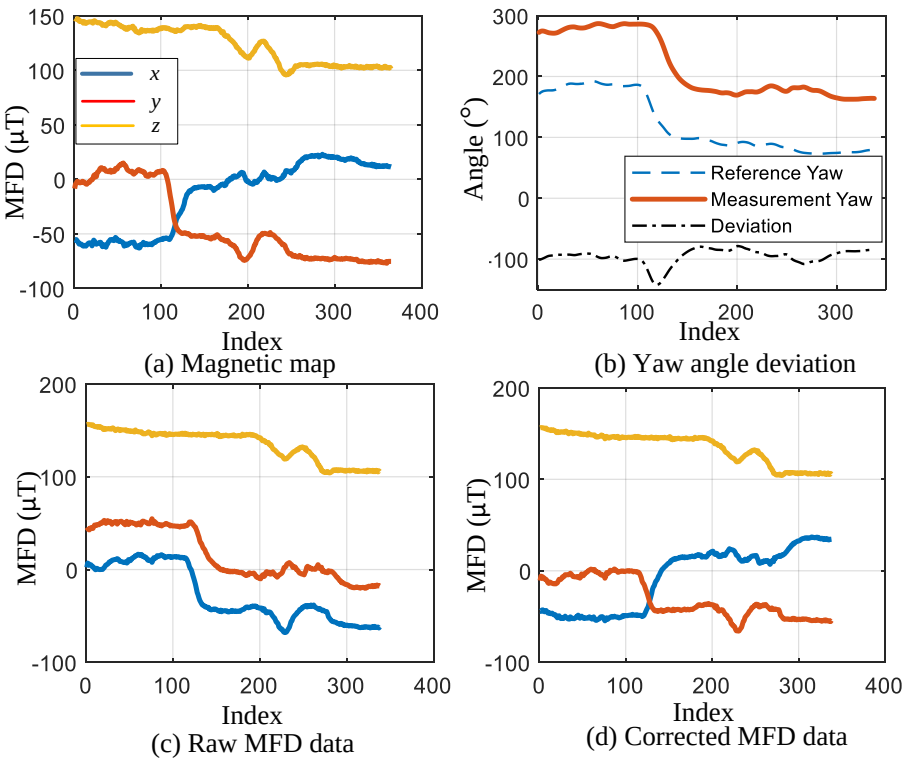

Figure 18: Illustration of magnetic field correction

As mentioned above, the orientation of the MTS and IMU are assumed to be the same only for the stationary walking phases. Thereby, the orientation of the MTS during the moving walking phases are estimated using linear interpolation using the orientation estimated during the stationary phases.

2.5.3 Position Correction

Instead of directly solely using double integration of the linear acceleration measurements to estimate location, Kalman Filter is introduced to fuse the inertial and geomagnetic information to obtain more reliable and accurate estimation. For this application (indoor position estimation), the estimation parameters are listed in Table 2. Where, $d_{i,t}$ and $\dot{d}^{b}_{i,t}$ are displacement and velocity bias respectively; $g_{i,k}$ is the position estimated from the MTS sensor, where the subscript $i = x, y, z$. The control input $\dot{d}_{i,t}$ is the corrected velocity estimated using Eq.13b.

Table 2: System parameter for position estimation using Kalman filter

System state: $\hat{\mathbf{x}}_t = \begin{bmatrix} d_{i,t} & \dot{d}^{b}_{i,t} \end{bmatrix}^{\mathrm{T}}$	**Control input:** $u_t = \dot{d}_{i,t}$	**Measurement:** $z_t = g_{i,t}$
Matrix coefficients: $[\mathbf{A}] = \begin{bmatrix} 1 & -\Delta t \\ 0 & 1 \end{bmatrix} [\mathbf{B}] = \begin{bmatrix} \Delta t \\ 0 \end{bmatrix} [\mathbf{H}] = [1 \quad 0]$		

Figure 19 illustrates the overall indoor localization algorithm using inertial and geomagnetic information. More specifically, with gravitation compensation method, the measurements of acceleration, angular velocity and geomagnetic field are utilized to estimate orientation, which can not only correct the geomagnetic field and magnetic tensor to conduct indoor localization with improved subsequence DTW, but also benefit the final

indoor localization. The acceleration measurements, orientation estimation and prior location estimation from geomagnetic information are integrated and fused with Kalman filter to conduct the indoor navigation.

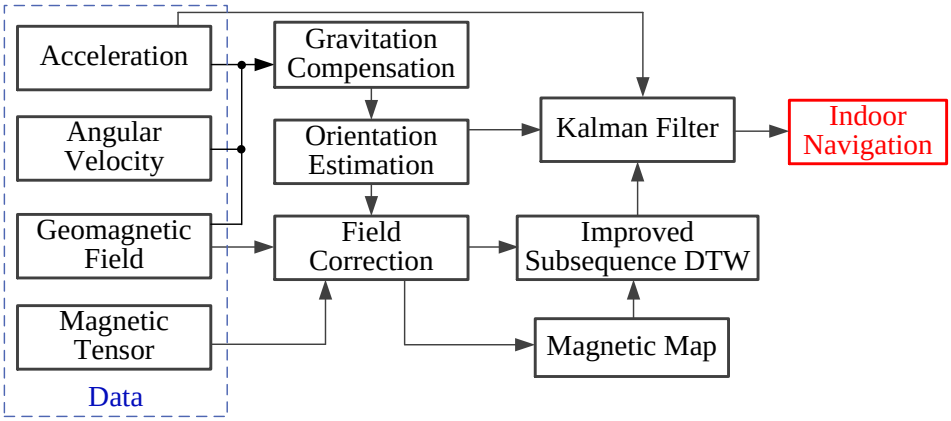

Figure 19: Flowchart illustrating overall indoor localization algorithm

Chapter 3. Sensing System Design and Implementation

To validate and demonstrate the algorithm of indoor navigation for the VIPs, a sensing system is designed, which includes individual sensor desgin, overall sensing system design and sensor calibration.

3.1 MTS Design

To validate and demonstrate the algorithm of indoor navigation for the VIPs, a sensing system is designed and implemented. Since the algorithm involves the inertial and geomagnetic information, the sensing system should be capable of measuring the acceleration, angular velocity, geomagnetic field and magnetic tensor. The measurement of the first three parameters can be simply obtained with an IMU, which contains an accelerometer, a gyroscope and a magnetometer. However, an MTS sensor is to be designed with proper parameters. A MTS consists of two orthogonal pairs of 3-axis magnetic sensors (BMC050) mounted at $\pm w/2$ (where w = 10 mm) from the *x* and *y* axes of the sensor local coordinate system as shown in Figure 20[22], is used to measure the magnetic tensor [**G**]. Because [**G**] defined in Eq. (16a) is symmetric and has the following property given in Eq. (16c), only five of its elements require calculation using Eq. (30) where $B_{i,x\pm}$ and $B_{i,y\pm}$ are the i^{th} MFD component from the sensor ($[\mathbf{G}]_{\pm}$) along *x* and *y* axes respectively:

$$\partial_x B_i = \frac{1}{w}\left(B_{i,x+} - B_{i,x-}\right) \text{ and } \partial_y B_j = \frac{1}{w}\left(B_{j,y+} - B_{j,y-}\right) \quad (30)$$

$$\text{where } i = x, y, z \text{ and } j = y, z$$

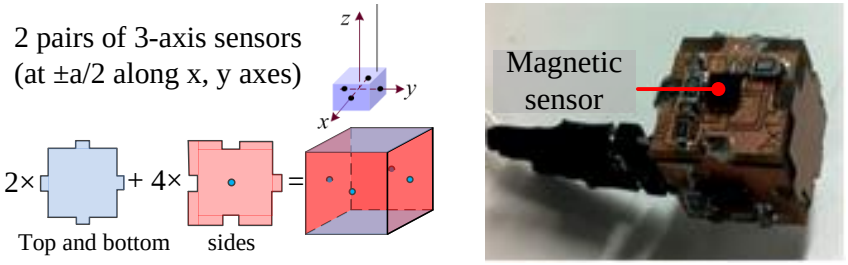

Figure 20: Schematics illustrating the MTS

3.2 Sensor Calibration

For efficient working of the designed sensing system, it is necessary to calibrate of all the sensors. The IMU and MTS needs to be warmed up for 2-3 minutes and calibrated before use. For the IMU, there is a slowly time-varying bias in inertial sensor measurement, which can be roughly eliminated by subtracting the mean of measurements when the sensor is stationary. A water level was used to make sure that the z axis of the IMU is exactly vertical during calibration. This should be done each time when the sensor is powered up. For MTS, since there are multiple magnetic sensors, misalignment is a major issue which need to be calibrated. Misalignment could be due to noise, geometric and positioning errors of all sensors. Calibration is done by moving the MTS in translational motion towards a permanent magnet in all 3-axis such that each sensor measures the MFD (denoted by $\mathbf{B}_i$ where i=1,2,3 and 4). The measurements $\mathbf{B}_j$ (where j=2,3 and 4) are related to $\mathbf{B}_1$ by

$$\left[\mathbf{H}_{j1}\right]\mathbf{B}_j = \mathbf{B}_1 \text{ and} \left[\mathbf{H}_{j1}\right] = \left[\mathbf{A}_{j1}\right]\left[\mathbf{T}_{j1}\right] \qquad (31a,b)$$

$\mathbf{A}_{j1}$ is 3 × 3 diagonal matrix accounting for relative scale factor between j^{th} and first sensor and $\mathbf{T}_{j1}$ is a 3 × 3 rotational matrix to describe $\mathbf{B}_j$ in $\mathbf{B}_1$ sensor coordinates. The measuring steps are repeated at N locations to calibrate $\mathbf{H}_{1i}$

$$\left[\mathbf{K}_i\right]=\left[\mathbf{B}_{i1}....\mathbf{B}_{ik}....\mathbf{B}_{iN}\right],\ \left[\mathbf{H}_{j1}\right]\left[\mathbf{K}_j\right]=\mathbf{B}_1 \tag{32a,b}$$

$\left[\mathbf{H}_{1i}\right]$ is given by

$$\left[\mathbf{H}_{1i}\right]=\left[\mathbf{K}_1\mathbf{K}_j^T\left[\mathbf{K}_j\mathbf{K}_j^T\right]^{-1}\right] \tag{33}$$

Apart from misalignment errors, Anomaly errors are to be calibrated. As all the magnetometers are put together using solder materials which are magnetic, this will affect the MFD measurements. For anomaly calibration, MTS need to be placed outside (no external magnetic anomalies), the measurements of the magnetic sensors in the MTS **T** consists of two components, MFD of the geomagnetic field $\mathbf{B}^G$ and internal magnetic anomalies $\mathbf{B}^A$ generated by the magnetic solder materials.

$$\mathbf{T}=\mathbf{B}^G+\mathbf{B}^A \tag{34}$$

In order to estimate $\mathbf{B}^A$, the MTS is placed outside with orientation shown in Figure 21. P2 and P3 can the positions when rotating 180° about *z* and *y* axis of the sensor frame. Assume internal magnetic anomalies $\mathbf{B}_1^G=\left[B_x^G\ \ B_y^G\ \ B_z^G\right]^T$ at P1, internal magnetic anomalies at P2 and P3 can be estimated with $\mathbf{B}_2^G=\left[-B_x^G\ \ -B_y^G\ \ B_z^G\right]^T$ and $\mathbf{B}_3^G=\left[-B_x^G\ \ B_y^G\ \ -B_z^G\right]^T$. Assume MFD measurements at P1, P2 and P3 are $\mathbf{T}_1$, $\mathbf{T}_2$ and $\mathbf{T}_3$ respectively, after applying Eq. (34) for each position, the internal magnetic anomalies BA can be estimated with Eq.(35).

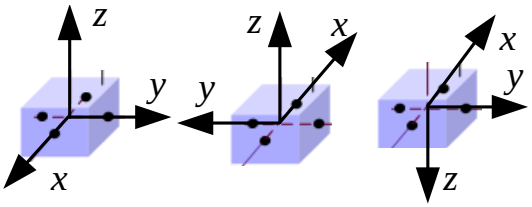

(a) P1 (b) P2 (c) P3

Figure 21: MTS Orientation for calibration

$$\mathbf{B}^A = \left[B_x^A \;\; B_y^A \;\; B_z^A \right]^T, \text{where } B_x^A = \left(T_{1x} + T_{2y} \right) / 2$$
$$B_y^A = \left(T_{1y} + T_{2y} \right) / 2, B_z^A = \left(T_{1z} + T_{3z} \right) / 2 \qquad (35a\sim e)$$

3.3 Sensing System Design

The design of the sensing system is illustrated in Figure 22 where the embedded system collects inertial and magnetic information and estimate the indoor location with the pre-loaded algorithm and magnetic map. The VIPs interact with the embedded system using the sound and vibration. The system is capable of refining and updating the pre-established magnetic map in the process of usage. The IMU is attached to the user's foot to correct the sensor drift with the characteristics of the human gait whereas the MTS is held in hand.

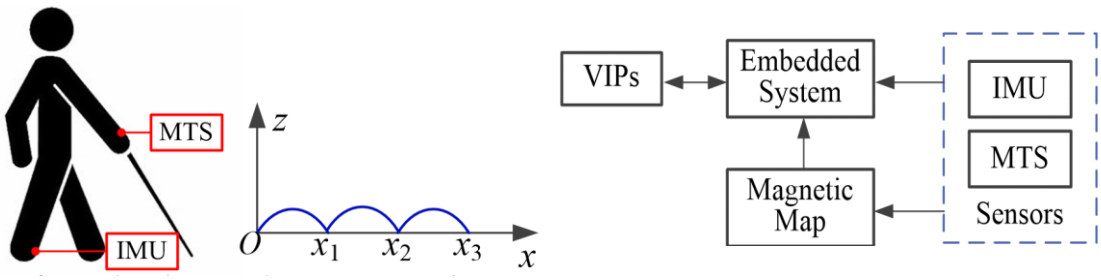

(a) Sensor Location (b) IMU Trajectory

Figure 22: Schematics illustrating the sensing system

Chapter 4. Experimental Demonstration and Validation

In order to demonstrate and validate the feasibility, accuracy and efficiency of the newly developed sensor fusion algorithms (Chapter 2) and design of the sensing system (Chapter 3), a prototype of the sensing system for indoor navigation is developed, which is followed by several experiments performed in the building.

4.1 Experimental Setup

A prototype of the sensing system designed for indoor navigation, which consists of an embedded system (Arduino Uno R3), an IMU, an SD data logger, an MTS and a battery, is developed as illustrated in Figure 23 With an inter-integrated circuit (I2C) communication protocol, the Arduino board acquires data from the IMU (GY-85) and MTS

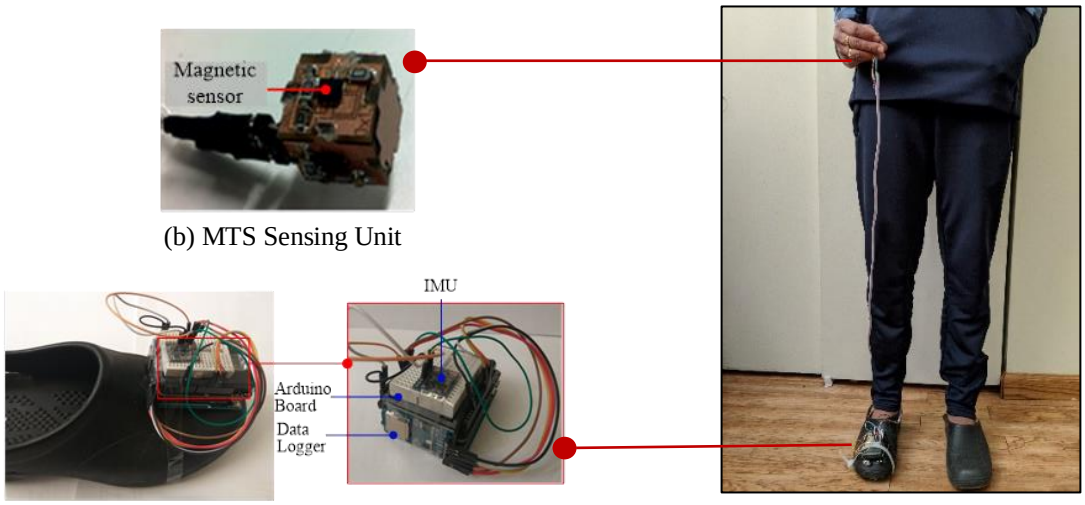

(b) MTS Sensing Unit

(b) IMU Sensing Unit

(c) Picture of User with the system

Figure 23: Prototype of Sensing System

and stores the data in an SD card. Figure 23(c) shows the overall system with IMU attached to one of the feet of the VIP and MTS sensor held in hand for data collection. Experiments

have been conducted using this prototype to validate the proposed algorithm using three routes in the university premises.

4.2 Experiment Results and Discussion

Several experiments were conducted in Trafton Science Center, Minnesota State University Mankato. Three indoor routes are selected, one of which is utilized to illustrate the feasibility and efficiency of certain critical operations of the algorithms. The experimental results are presented in this section, which is followed by the discussion from the observations.

(a) Route map (b) Pictures of the route

Figure 24: Indoor Route Map

Assume the VIP enters the building through the north entrance (red circle) and needs to go to Room C127 (red star) with the route (total distance 119m) map and pictures shown in Figure 24 using the designed prototype sensing system.

The result analysis follows the algorithm discussed in sections of Chapter 2. Firstly, a comparison between two cases, without and with the use of ZVU method is made. In the first case shown in Figure 25 a huge drift in position estimation can be observed with pure integration of angular velocity and acceleration data where, ZVU and velocity drift correction is not implemented. In the latter case, shown in Figure 26 use of ZVU and drift correction does improve the result capturing all the motion and stationary periods. However, this position estimation is not accurate and has to be improved to match with the route considered in Figure 24.

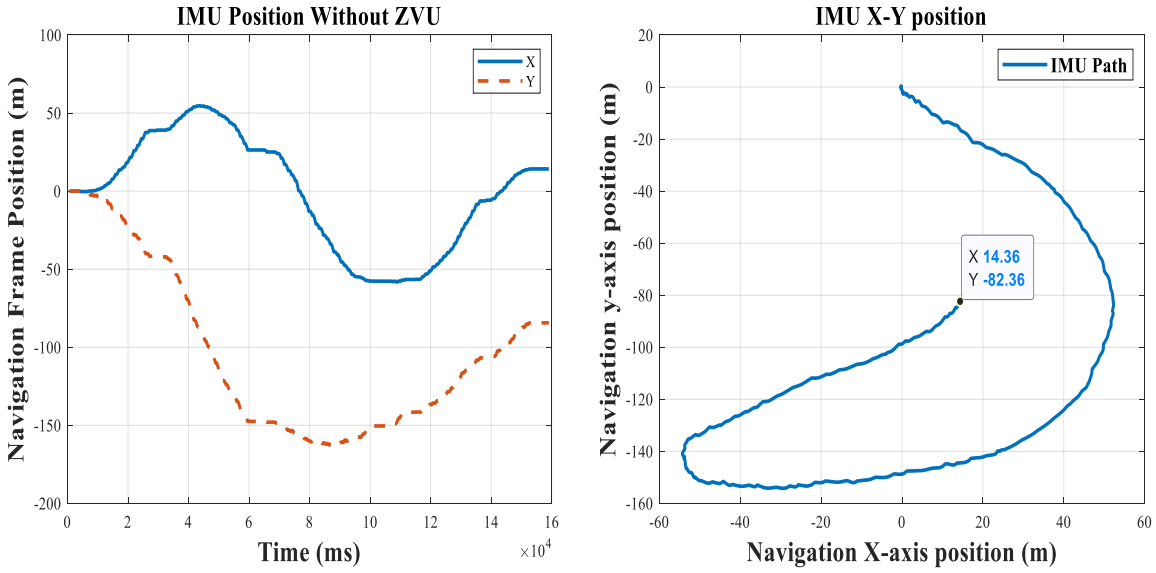

Figure 25: Estimation without ZVU and Drift Correction

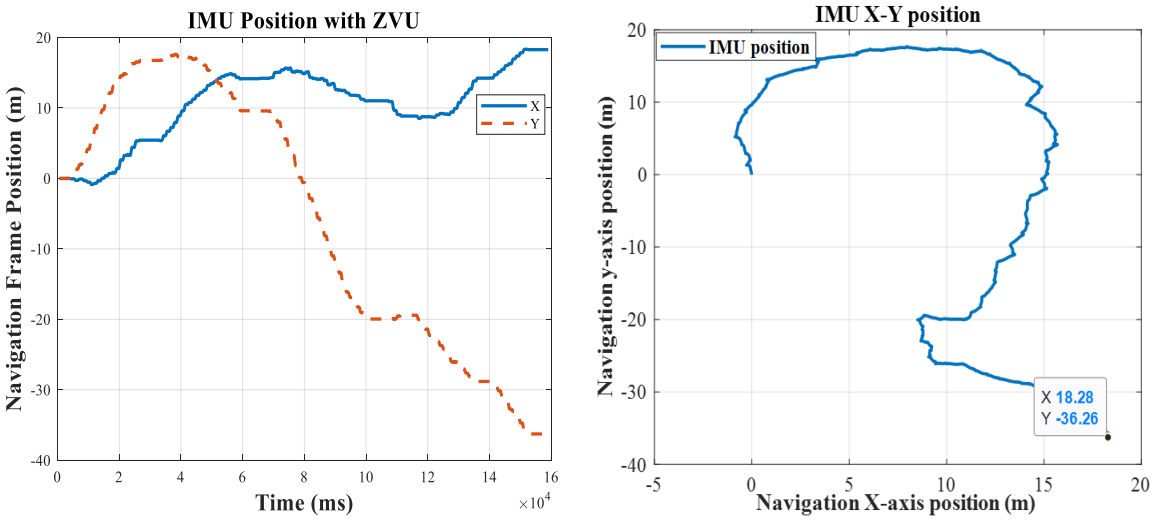

Figure 26: Estimation with ZVU and Drift Correction

ZVU method does capture the motion of the user, however, a closer look at the four quaternions representing orientation from Figure 27(a) ,a pure integration for orientation would result in a drift, consequently effecting the position estimation. Figure 27(b) shows the drift corrected quaternions using pitch and roll angular rate error correction using accelerometer data during the stationary intervals as explained in section 2.2.2.

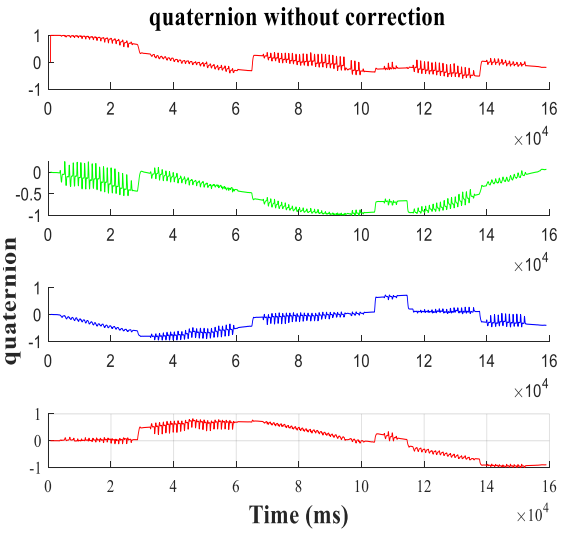

Figure 27(a): No Pitch and Roll Correction

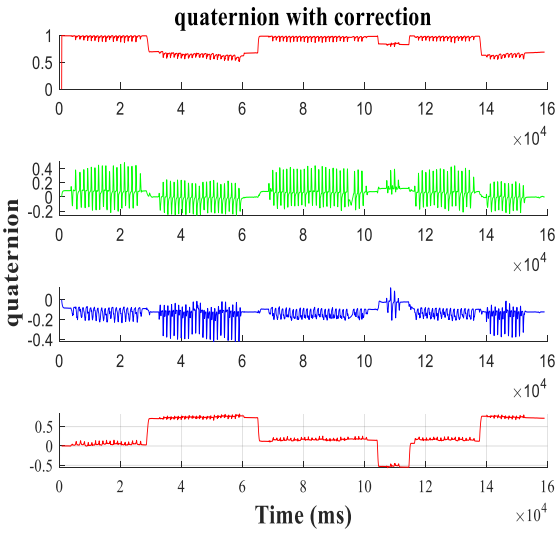

Figure 27(b): Pitch and Roll Corrected

A sufficient gain would ensure pitch and roll representing quaternions to correct during stationary periods. Although accelerometer data cannot be used for yaw correction, pitch and roll correction attributes to the change in yaw due to the dependency of all four quaternions. Figure 28 shows a significant improvement in position estimation after pitch and roll correction and Table 3 shows error comparison of non ZVU, ZVU and pitch, roll corrected position estimations.

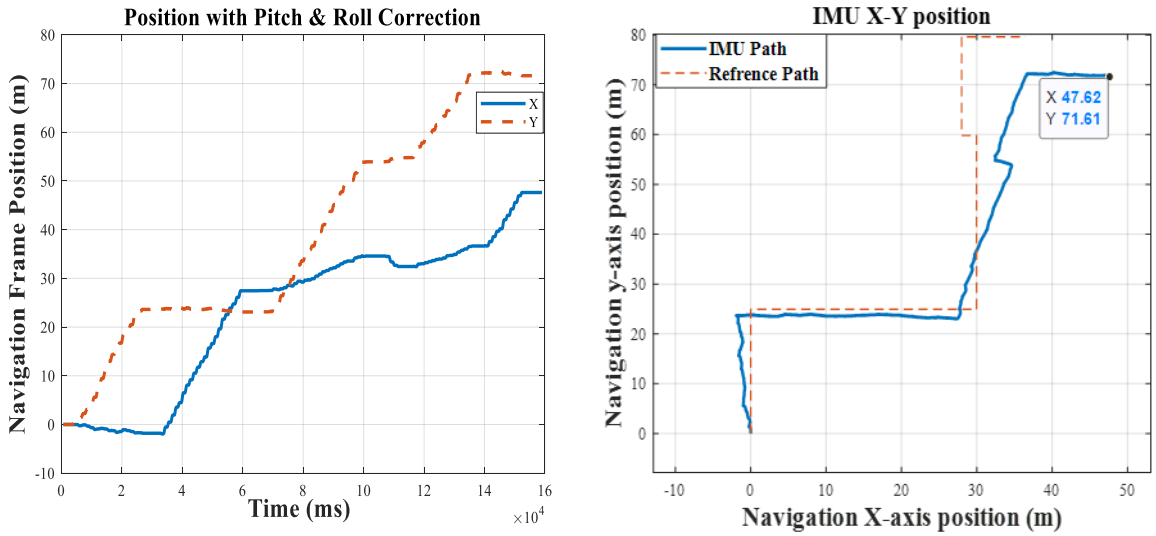

Figure 28: Pitch and Roll Corrected Position

Table 3: Position Error Comparison using ZVU, Pitch and Roll correction methods

Method	Error X-axis (m)	Error Y-axis (m)
No ZVU	20.64	162.36
ZVU	16.7	116.26
(ZVU)+(Pitch & Roll corrected)	12.62	8.59

Orientation correction for motion periods can also be done, however, due to the presence of external accelerations apart from gravity, the use of raw accelerometer data

would contaminate the position. Figure 29(a) and (b) show a comparison between raw data versus low pass filtered accelerometer data for correction during motion and stationary periods and Table 4 gives error comparison. However, the gains can be different for both periods.

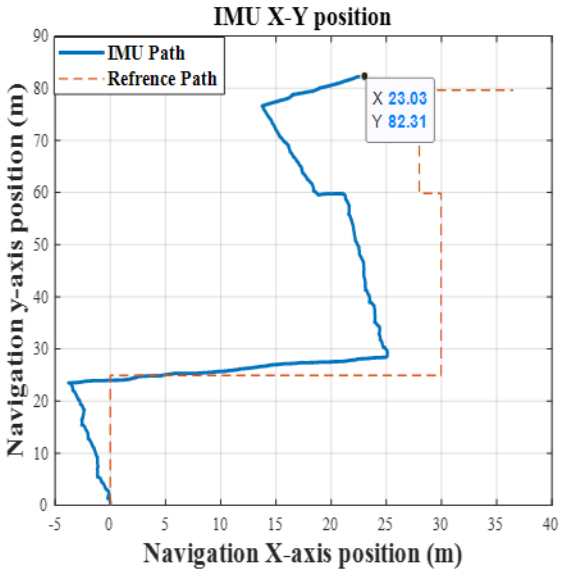

Figure 29(a): Raw Data for Correction

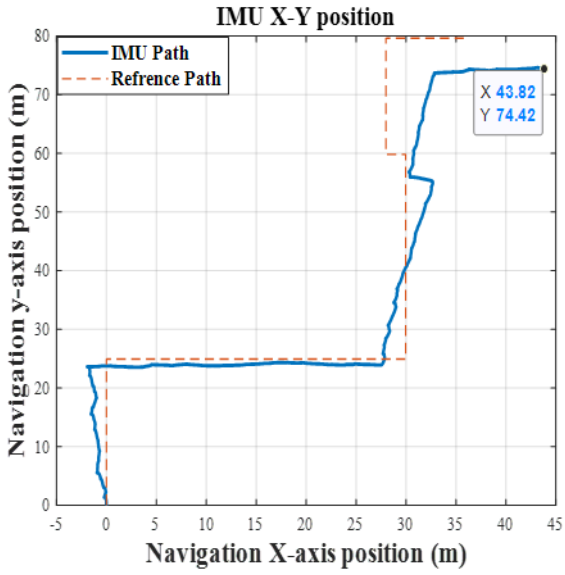

Figure 29(b): Low pass Filtered Data for Correction

Table 4: Position Error Comparison for Raw and Filtered Data for Orientation Correction

Method	Error X-axis (m)	Error Y-axis (m)
Raw Data	12.96	2.31
Filtered	8.83	5.58

A deviation of more than 8m observed with respect to x-axis is attributed to an error in yaw estimation. Figure 30 shows yaw corrected position estimation, where Geo-magnetic information is used to correct the yaw for instances with relatively constant gradient.

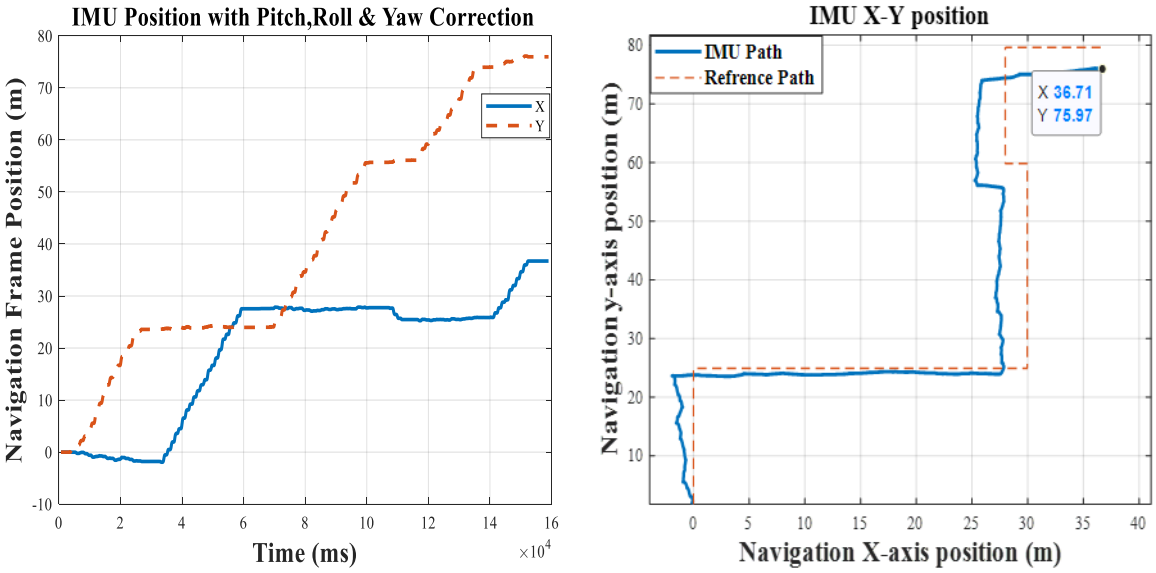

Figure 30: Yaw Corrected Position

From all the error corrections used for position estimation using IMU it can be observed that the error is reduced at each stage. However, a deviation from the reference path is still observed from Figure 30 which requires an improvement using MTS sensor.

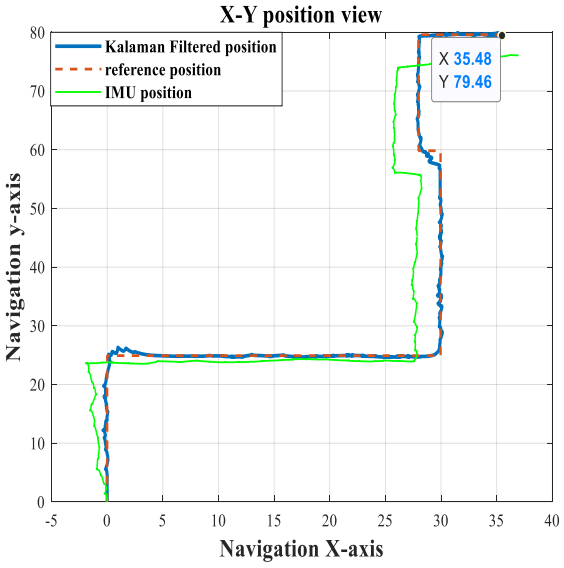

Figure 31: Comparison of Results

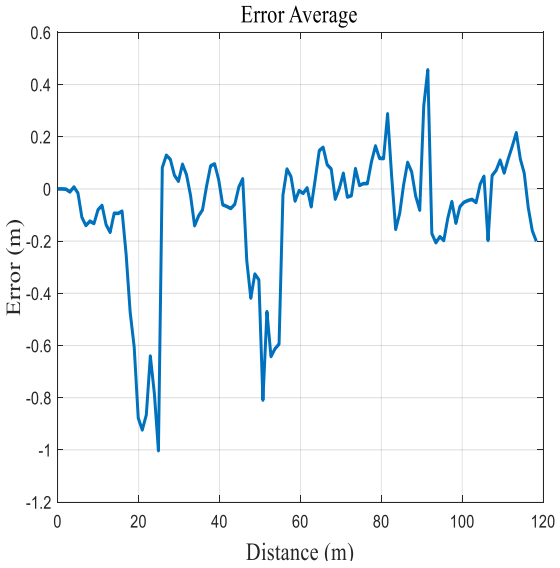

Figure.32: Error Average

Table 5: Comparison of Results

Method	Error X-axis (m)	Error Y-axis (m)
IMU	0.71	4.07
Kalman (IMU+MTS)	0.48	0.54

As the reference magnetic map generated by MTS is a representation of route co-ordinates, position of a measurement instant would refer to position of a matching instant of reference map. Figure 31 compares the results estimated using IMU and KF filter with the actual route and Table 5 lists the error of IMU and KF with reference to reference route.

The average errors of KF filter results for 4 trials plotted in Figure 32 shows an average localization error for the whole route of 0.092 m, concluding that the position is much better than sole use of IMU.

The additional experiments using Route map 2 and 3 were conducted to validate the proposed method. In the first case, the VIP is assumed to take a round trip of 98m from N135 of Trafton North in a rectangular shape with route map as shown in Figure 33(a). In the latter experiment, the VIP is assumed to enter the building through the Trafton east entrance (red circle) and needs to go to Room N186 (red star) with the route (total distance 105m) map shown in Figure 34(a). Similarly, the average errors of KF filter results for 4 trials using Route map 2 and 3 are shown in Figure 35(a) and (b) with the average localization error for the whole route are 0.186m and 0.058m respectively.

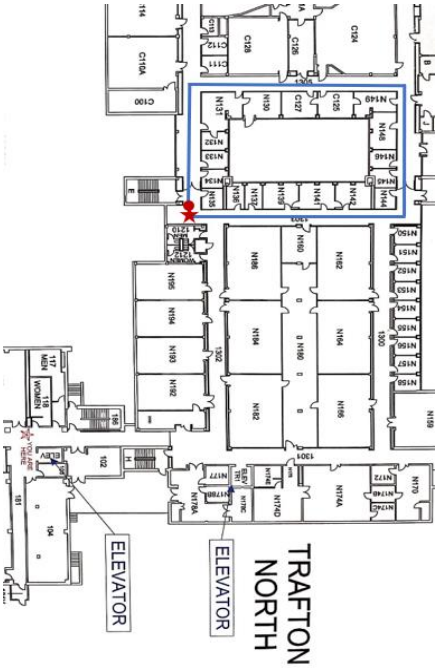

Figure 33(a): Route Map 2

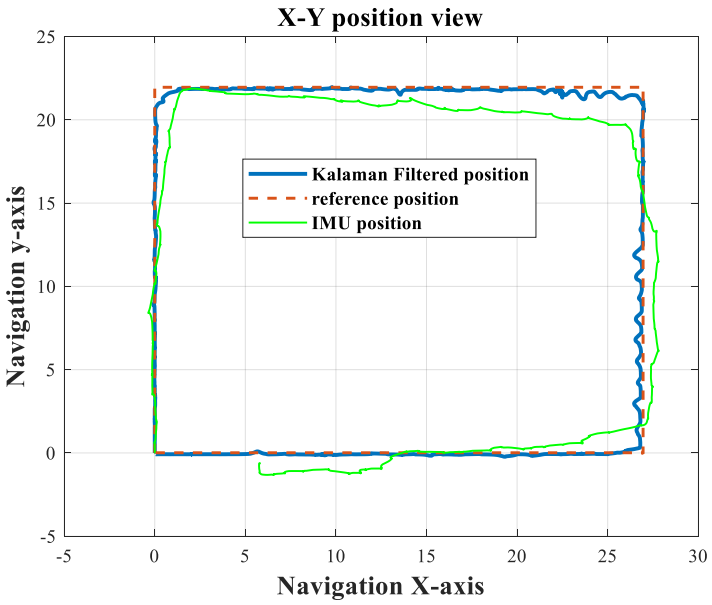

Figure 33(b): Route 2 Result Comparison

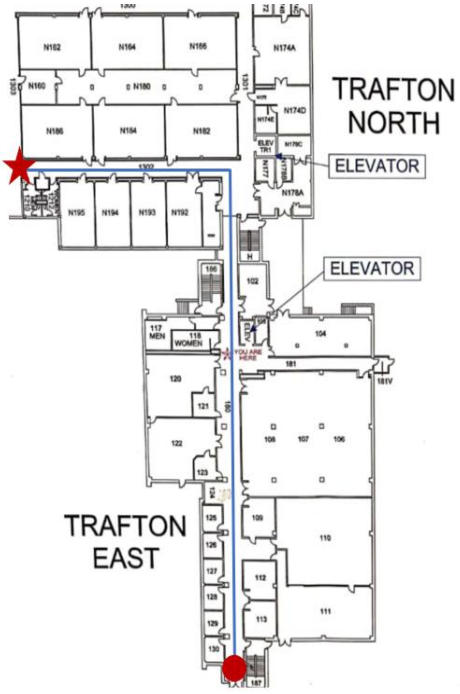

Figure 34(a): Route Map 3

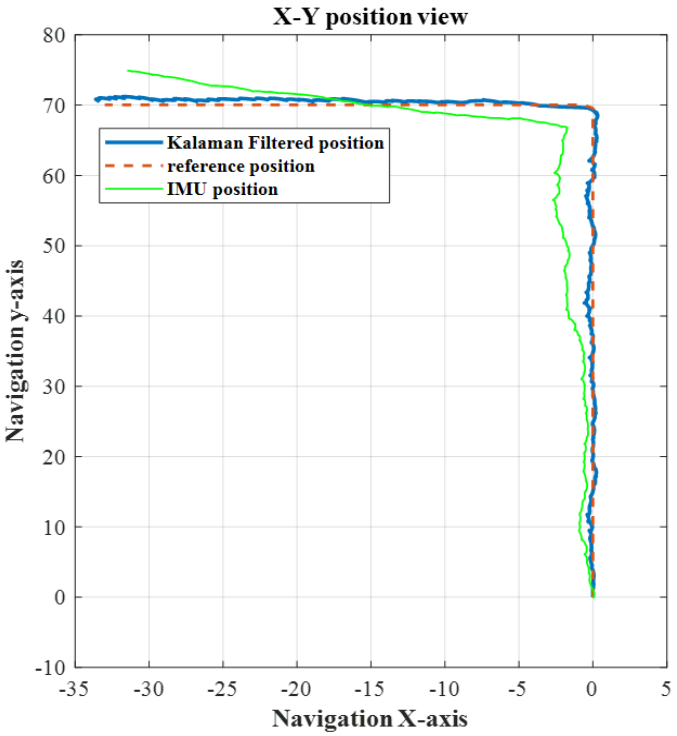

Figure 34(b): Route 3 Result Comparison

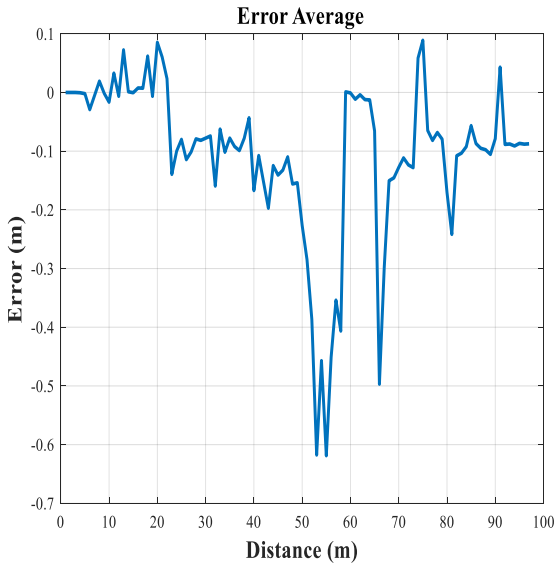

Figure 35(a): Route Map 2 Error Analysis

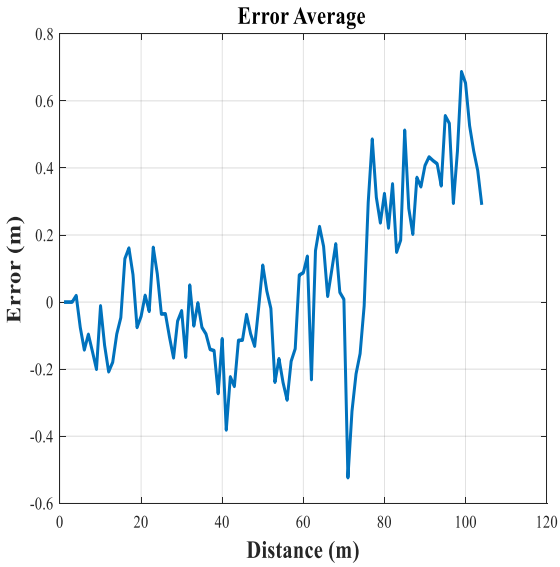

Figure 35(b): Route Map 3 Error Analysis

Chapter 5. Conclusion and Future Work

A sensing system capable of accurately navigating a VIP indoor is presented. Inertial and geo-magnetic information is utilized in every possible way to correct any error in localization. Human gait characteristics are used to eliminate the accumulated drift by IMU and distorted MFD of surrounding spatial information is utilized by MTS. An interaction between IMU and MTS is observed for both orientation and position estimations using sensor fusion algorithms. The experiments using three different indoor routes with the distance of 119m, 98m and 105m were conducted to demonstrate and validate the designed algorithms and sensing system. Relatively large errors are observed at the corner locations which is similar for route 2 and route 3. The error averages of all three routes is observed to be 0.092m, 0.186m and 0.058m respectively, which successfully demonstrate the accuracy and efficiency of the newly designed sensing system for the VIP indoor navigation.

Even though the designed system can guide the VIPs indoor, there are several problems unsolved, which motivates the future improvements of the existing algorithms and sensing systems. Several possible and potential improvements are listed as followed.

- For the newly designed system, the MTS and IMU are attached to different part of human body, which results in the difficulty of obtaining the orientation of the MTS. To solve this problem, another IMU will be introduced to attach to the MTS.
- A more accurate IMU will be introduced to improve the orientation and location estimation.

- Instead of using the standard Kalman filter, the extended Kalman filter has the potential to improve the accuracy of the location estimation.
- The potential indoor navigation applications with the routes containing free space and stair climbing instead of the corridors will be explored using the newly designed sensing system.

References

[1] “MEMS Gyroscope Provides Precision Inertial Sensing in Harsh, High Temperature Environments,” *MEMS Gyroscope Provides Precision Inertial Sensing in Harsh, High Temperature Environments | Analog Devices*. [Online]. Available: https://www.analog.com/en/technical-articles/mems-gyroscope-provides-precision-inertial-sensing.html. [Accessed: 05-Mar-2020].

[2] “Sonic Nirvana: Using MEMS Accelerometers as Acoustic Pickups in Musical Instruments,” *Using MEMS Accelerometers as Acoustic Pickups in Musical Instruments | Analog Devices*. [Online]. Available: https://www.analog.com/en/analog-dialogue/articles/mems-accelerometers-as-acoustic-pickups.html#. [Accessed: 05-Mar-2020].

[3] Global Data on Visual Impairment. [Online]. Available: https://www.who.int/blindness/publications/globaldata/en/. [Accessed: 25-Feb-2020].

[4] A. J. Davison, I. D. Reid, N. D. Molton, and O. Stasse, “MonoSLAM: Real-Time Single Camera SLAM,” *IEEE Transactions on Pattern Analysis and Machine Intelligence*, vol. 29, no. 6, pp. 1052–1067, 2007.

[5] H. Strasdat, J. M. M. Montiel and A. J. Davison, "Real-time monocular SLAM: Why filter?," *IEEE International Conference on Robotics and Automation*, Anchorage, AK, 2010, pp. 2657-2664.

[6] S. Treuillet and E. Royer, “Outdoor/indoor Vision-Based Localization For Blind Pedestrian Navigation Assistance,” *International Journal of Image and Graphics*, vol. 10, no. 04, pp. 481–496, 2010.

[7] B. Walther-Franks, R. Malaka, "Evaluation of an augmented photograph-based pedestrian navigation system" in *Smart Graphics*, Springer, pp. 94-105, 2008.

[8] N. Yazdi, F. Ayazi and K. Najafi, "Micromachined inertial sensors," in *Proceedings of the IEEE*, vol. 86, no. 8, pp. 1640-1659, Aug. 1998.

[9] E. R. Bachmann, X. Yun and A. Brumfield, "Limitations of Attitude Estimnation Algorithms for Inertial/Magnetic Sensor Modules," in *IEEE Robotics & Automation Magazine*, vol. 14, no. 3, pp. 76-87, Sept. 2007.

[10] M. Kok, J. D. Hol, and T. B. Schön, "Using Inertial Sensors for Position and Orientation Estimation," *Foundations and Trends® in Signal Processing*, vol. 11, no. 1-2, pp. 1–153, 2017.

[11] R. Cechowicz, "Bias Drift Estimation for MEMS Gyroscope Used in Inertial Navigation," *Acta Mechanica et Automatica*, vol. 11, no. 2, pp. 104–110, Jan. 2017.

[12] Y. Javed, Z. Khan, and S. Asif, "Evaluating Indoor Location Triangulation Using Wi-Fi Signals," *Advances in Internet, Data and Web Technologies. Lecture Notes on Data Engineering and Communications Technologies*, vol 29, pp. 180–186, 2019.

[13] F. Seco, C. Plagemann, A. R. Jiménez and W. Burgard, "Improving RFID-based indoor positioning accuracy using Gaussian processes," 2010 *International Conference on Indoor Positioning and Indoor Navigation*, Zurich, 2010, pp. 1-8.

[14] J. Na, "The Blind Interactive Guide System Using RFID-Based Indoor Positioning System," *Lecture Notes in Computer Science Computers Helping People with Special Needs*, vol. 4061, pp. 1298–1305, 2006.

[15] V. Kulyukin, C. Gharpure, J. Nicholson and S. Pavithran, "RFID in robot-assisted indoor navigation for the visually impaired," 2004 *IEEE/RSJ International Conference on Intelligent Robots and Systems (IROS) (IEEE Cat. No.04CH37566)*, Sendai, 2004, pp. 1979-1984, vol.2.

[16] D. López-De-Ipiña, T. Lorido, and U. López, "BlindShopping: Enabling Accessible Shopping for Visually Impaired People through Mobile Technologies," *In Proceedings of the 9th International Conference on Smart Homes and Health Telematics*, vol 6719, pp. 266–270, 2011.

[17] D. López-De-Ipiña, T. Lorido, and U. López, "Indoor Navigation and Product Recognition for Blind People Assisted Shopping," *In Proceedings of the 3rd International Workshop on Ambient Assisted Living*, pp. 33–40, Jun. 2011.

[18] Sonnenblick, Y "An Indoor Navigation System for Blind Individuals," *In Proceedings of the 13th Annual Conference on Technology and Persons with Disabilities*, pp. 215–224, 1998.

[19] Chunhan Lee et al., "Indoor positioning system based on incident angles of infrared emitters," *30th Annual Conference of IEEE Industrial Electronics Society*, 2004. IECON 2004, Busan, South Korea, 2004, pp. 2218-2222 vol. 3.

[20] L. Ran, S. Helal and S. Moore, "Drishti: an integrated indoor/outdoor blind navigation system and service," *Proceedings of the Second IEEE Annual Conference on Pervasive Computing and Communications*, Orlando, FL, USA, 2004, pp. 23-30.

[21] K. P. Subbu, B. Gozick, and R. Dantu, "LocateMe," *ACM Transactions on Intelligent Systems and Technology*, vol. 4, no. 4, pp. 1–27, Sep. 2013.

[22] K.-M. Lee, M. Li, and C.-Y. Lin, “Magnetic Tensor Sensor and Way-Finding Method Based on Geomagnetic Field Effects With Applications for Visually Impaired Users,” *IEEE/ASME Transactions on Mechatronics*, vol. 21, no. 6, pp. 2694–2704, 2016.

[23] P. Aggarwal, Z. Syed, X. Niu, and N. El-Sheimy, “A Standard Testing and Calibration Procedure for Low Cost MEMS Inertial Sensors and Units,” *Journal of Navigation*, vol. 61, no. 2, pp. 323–336, 2008.

[24] K. Seifert and O. Camacho, “Implementing Positioning Algorithms Using Accelerometers.” Application Note AN3397, Freescale Semiconductor, Feb. 2007.

[25] Ö. Bebek et al., "Personal Navigation via High-Resolution Gait-Corrected Inertial Measurement Units," in *IEEE Transactions on Instrumentation and Measurement*, vol. 59, no. 11, pp. 3018-3027, Nov. 2010.

[26] R. E. Kalman, “A New Approach to Linear Filtering and Prediction Problems,” *Journal of Basic Engineering*, vol. 82, no. 1, p. 35, 1960.

[27] E. Foxlin, "Inertial head-tracker sensor fusion by a complementary separate-bias Kalman filter," *Proceedings of the IEEE 1996 Virtual Reality Annual International Symposium*, Santa Clara, CA, USA, 1996, pp. 185-194.

[28] H. Luinge, P. Veltink, and C. Baten, “Estimating orientation with gyroscopes and accelerometers,” *Technology and Health Care*, vol. 7, no. 6, pp. 455–459, Jan. 1999.

[29] J. L. Marins, Xiaoping Yun, E. R. Bachmann, R. B. McGhee and M. J. Zyda, "An extended Kalman filter for quaternion-based orientation estimation using MARG

sensors," *Proceedings 2001 IEEE/RSJ International Conference on Intelligent Robots and Systems,* Maui, HI, USA, 2001, pp. 2003-2011 vol.4.

[30] Kim, N.; Kim, Y. Indoor Positioning System with IMU, Map Matching and Particle Filter. In *Recent Advances in Electrical Engineering and Control Applications; Springer*: Berlin, Germany, 2015; pp. 41–47.

[31] H. Fourati, "Heterogeneous Data Fusion Algorithm for Pedestrian Navigation via Foot-Mounted Inertial Measurement Unit and Complementary Filter," in *IEEE Transactions on Instrumentation and Measurement*, vol. 64, no. 1, pp. 221-229, Jan. 2015.

[32] R. Mahony, T. Hamel and J. Pflimlin, "Nonlinear Complementary Filters on the Special Orthogonal Group," in *IEEE Transactions on Automatic Control*, vol. 53, no. 5, pp. 1203-1218, June 2008.

[33] K. Feng, J. Li, X. Zhang, C. Shen, Y. Bi, T. Zheng, and J. Liu, "Correction: A New Quaternion-Based Kalman Filter for Real-Time Attitude Estimation Using the Two-Step Geometrically-Intuitive Correction Algorithm. Sensors 2017, 17, 2146," *Sensors*, vol. 17, no. 11, p. 2530, Mar. 2017.

[34] D. Choukroun, I. Y. Bar-Itzhack and Y. Oshman, "Novel quaternion Kalman filter," in IEEE Transactions on Aerospace and Electronic Systems, vol. 42, no. 1, pp. 174-190, Jan. 2006.

[35] V. Renaudin and C. Combettes, "Magnetic, Acceleration Fields and Gyroscope Quaternion (MAGYQ)-Based Attitude Estimation with Smartphone Sensors for Indoor Pedestrian Navigation," *Sensors*, vol. 14, no. 12, pp. 22864–22890, Feb. 2014.

[36] B. Barshan and H. Durrant-Whyte, “An Inertial Navigation System for a Mobile Robot,” *IFAC Proceedings Volumes,* vol. 26, no. 1, pp. 54–59, 1993.

[37] H. J. Luinge and P. H. Veltink, “Measuring orientation of human body segments using miniature gyroscopes and accelerometers,” *Medical & Biological Engineering & Computing*, vol. 43, no. 2, pp. 273–282, 2005.

[38] D. Jurman, M. Jankovec, R. Kamnik, and M. Topič, “Calibration and data fusion solution for the miniature attitude and heading reference system,” *Sensors and Actuators A: Physical*, vol. 138, no. 2, pp. 411–420, 2007.

[39] M. Haid and J. Breitenbach, “Low cost inertial orientation tracking with Kalman filter,” *Applied Mathematics and Computation*, vol. 153, no. 2, pp. 567–575, 2004.

[40] D. Roetenberg, H. J. Luinge, C. T. M. Baten and P. H. Veltink, "Compensation of magnetic disturbances improves inertial and magnetic sensing of human body segment orientation," in *IEEE Transactions on Neural Systems and Rehabilitation Engineering*, vol. 13, no. 3, pp. 395-405, Sept. 2005.

[41] D. Gebre-Egziabher, R. C. Hayward and J. D. Powell, "Design of multi-sensor attitude determination systems," in IEEE Transactions on Aerospace and Electronic Systems, vol. 40, no. 2, pp. 627-649, April 2004.

[42] P. Nguyen Ho Quoc, K. Hee-Jun, S. Young-Soo, and R. Young-Sik, “A DCM Based Orientation Estimation Algorithm with an Inertial Measurement Unit and a Magnetic Compass,” *Journal of Universal Computer Science*, vol. 15, no. 4, pp. 859–876, Feb. 2009.

[43] S. O. H. Madgwick, A. J. L. Harrison and R. Vaidyanathan, "Estimation of IMU and MARG orientation using a gradient descent algorithm," *IEEE International Conference on Rehabilitation Robotics*, Zurich, 2011, pp. 1-7.

[44] Y. Cui, Y. Zhang, Y. Huang, Z. Wang, and H. Fu, "Novel WiFi/MEMS Integrated Indoor Navigation System Based on Two-Stage EKF," *Micromachines*, vol. 10, no. 3, p. 198, March 2019.

[45] Y. Li, Y. Zhuang, H. Lan, P. Zhang, X. Niu, and N. El-Sheimy, "WiFi-Aided Magnetic Matching for Indoor Navigation with Consumer Portable Devices," *Micromachines*, vol. 6, no. 6, pp. 747–764, Jun 2015.

[46] Y. Zhang, J. Tan, Z. Zeng, W. Liang and Y. Xia, "Monocular camera and IMU integration for indoor position estimation," *36th Annual International Conference of the IEEE Engineering in Medicine and Biology Society*, Chicago, IL, 2014, pp. 1198-1201.

[47] A. Poulose, O. S. Eyobu and D. S. Han, "An Indoor Position-Estimation Algorithm Using Smartphone IMU Sensor Data," in IEEE Access, vol. 7, pp. 11165-11177, 2019.

[48] G. Hasan, K. Hasan, R. Ahsan, T. Sultana, and R. C. Bhowmik, "Evaluation of a Low-Cost MEMS IMU for Indoor Positioning System ," *International Journal of Emerging Science and Engineering*, vol. 1, no. 11, Sept. 2013.

[49] C. Lu, H. Uchiyama, D. Thomas, A. Shimada, and R.-I. Taniguchi, "Indoor Positioning System Based on Chest-Mounted IMU," *Sensors*, vol. 19, no. 2, p. 420, Jan 2019.

[50] J. An, L. Yang, and J. Lee, “Three-dimensional indoor location estimation using single inertial navigation system with linear regression,” *Measurement Science and Technology*, vol. 30, no. 10, p. 105101, Dec. 2019.

[51] H. Hellmers, A. Norrdine, J. Blankenbach and A. Eichhorn, "An IMU/magnetometer-based Indoor positioning system using Kalman filtering," *International Conference on Indoor Positioning and Indoor Navigation*, Montbeliard-Belfort, 2013, pp. 1-9.

[52] M. Kok, N. Wahlström, T. B. Schön and F. Gustafsson, "MEMS-based inertial navigation based on a magnetic field map," *2013 IEEE International Conference on Acoustics, Speech and Signal Processing*, Vancouver, BC, 2013, pp. 6466-6470.

[53] Seong-Eun Kim, Yong Kim, Jihyun Yoon and Eung Sun Kim, "Indoor positioning system using geomagnetic anomalies for smartphones," *2012 International Conference on Indoor Positioning and Indoor Navigation (IPIN)*, Sydney, NSW, 2012, pp. 1-5.

[54] J. Kuang, X. Niu, P. Zhang, and X. Chen, “Indoor Positioning Based on Pedestrian Dead Reckoning and Magnetic Field Matching for Smartphones,” *Sensors*, vol. 18, no. 12, p. 4142, Nov 2018.

[55] PaulsenDesign, “World globe,” 01-Sep-2015. [Online]. Available: https://www.turbosquid.com/3d-models/3d-world-globe/956761. [Accessed: 10-Jul-2020].

[56] G. Welch and G. Bishop, “An Introduction to the Kalman Filter,” in *SIGGRAPH 2001: August 12-17, 2001, Los Angeles, California*, New York: ACM, 2001.